Macromolecules
ARTICLE

Macromolecules **2010**, *43*, 2605–2621 **2605**
DOI: 10.1021/ma902507d

Carbon Dioxide Solubility in Three Fluorinated Polyimides Studied by Molecular Dynamics Simulations

Sudharsan Pandiyan,[†,‡] David Brown,*[,†] Sylvie Neyertz,[†] and N. F. A. van der Vegt[‡,§]

[†]*LMOPS-UMR CNRS 5041, University of Savoie, Bât IUT, 73376 Le Bourget-du-Lac Cedex, France, and* [‡]*Max-Planck-Institute for Polymer Research, Ackermannweg 10, 55128 Mainz, Germany.* [§]*Current address: Center of Smart Interfaces, Technical University of Darmstadt, Petersenstrasse 32, 64287 Darmstadt, Germany.*

Received November 13, 2009; Revised Manuscript Received January 18, 2010

ABSTRACT: Fluorinated polyimides are interesting polymer materials for gas separation applications because of their good mechanical, thermal, and transport properties. We have performed molecular dynamics simulations (MD) of CO_2 sorption and desorption in three fluorinated polyimides: 6FDA-6FpDA, 6FDA-6FmDA, and 6FDA-DAM. These polyimides are known to vary significantly in their gas permeation properties. A stepwise procedure was used to insert CO_2 molecules into the previously prepared polymer matrices in order to mimick the experimental procedure of progressive loading and to avoid the necessity of preswelling the samples. An iterative technique was then used to estimate the vapor pressure of CO_2 that would have to be applied in order to obtain the imposed uptake. The resulting sorption isotherms are found to be in relatively good agreement with their respective experimental curves, and the trend in solubility was reproduced (6FDA-DAM > 6FDA-6FpDA > 6FDA-6FmDA). Desorption isotherms were also calculated starting from systems corresponding to an applied pressure of 60 bar. Hysteresis was evident even upon immediate unloading. Changes in volume, void space, potential energies, etc., have been characterized and compared to experimental data and to theories of gas sorption and plasticization in glassy polymers.

1. Introduction

Carbon dioxide (CO_2) separation has become a challenging task in many industries. It is generally accepted that the increased emission of CO_2 to the atmosphere is an important reason for global warming.[1] There are different techniques to separate CO_2 from gas mixtures such as physical adsorption,[2−8] chemical adsorption,[6,9−16] low-temperature distillation,[17,18] and membrane separation.[19−28] The latter technique made the transition from the laboratory to commercial ventures in the early 1980s. Indeed, some dense glassy polymers have interesting features such as a fairly low cost, easy installation, high selectivities for specific permeants, and a high solubility for CO_2.[29]

The most basic requirements for polymer membranes to efficiently transport gas molecules are high permeation rates (or productivities) and selectivities (or separation efficiencies). Permeability P is the rate of transport for the penetrant through the membrane defined as the product of its solubility coefficient S and its diffusion coefficient D (eq 1):

$$P = SD \tag{1}$$

In eq 1, S is a thermodynamic parameter which can be obtained from the sorption isotherm (if C is the penetrant concentration and p is the partial pressure, then $S = C/p$). D is a kinetic parameter determined by chain packing and the mobility of the polymer chain segments as well as by the size and shape of the penetrant molecules. When applied to a gas mixture, the selectivity of the polymer membrane for gas A over gas B, $\alpha_{A/B}$ (also called permselectivity), is the ratio of their pure gas permeabilities (eq 2):

$$\alpha_{A/B} = \frac{P_A}{P_B} = \left(\frac{D_A}{D_B}\right)\left(\frac{S_A}{S_B}\right) \tag{2}$$

An important property of nonporous dense membranes is that permeants of similar sizes and diffusion coefficients can be separated if their solubilities differ to a large extent. This is especially important for CO_2 separation applications as carbon dioxide exhibits much higher solubilities in dense polymers than other light gases.[30,31]

The transport of gases through polymer membranes can generally be described by a solution-diffusion mechanism.[32−36] Transport occurs when gas molecules in an upstream compartment enter the polymer matrix, diffuse across it, and finally desorb on a downstream gas compartment.[37] However, it is well-known that CO_2 transport in glassy polymers often results in plasticization effects and that the performance of the membrane can be significantly altered. For example, in CO_2/CH_4 gas separations, the polymer swells upon sorption of CO_2 accelerating the permeation of CH_4 and decreasing the permselectivity.[38]

Fluorinated polyimides are interesting polymer materials for gas separation applications because of their good mechanical, thermal, and transport properties.[39−58] They also exhibit an acceptable resistance to plasticization.[41,42,59] In the present paper, we perform molecular dynamics (MD) simulations of CO_2 sorption and desorption in three fluorinated polyimides in order to characterize CO_2 solubility and plasticizing effects as a function of the polymer structure. The three polyimides under study are (a) poly{4,4′-(2,2,2-trifluoro-1-(trifluoromethyl)ethane-1,1-diyl)dianiline}-*alt*-{5,5′-(2,2,2-trifluoro-1-(trifluoromethyl)ethane-1,1-diyl)bis(isobenzofuran-1,3-dione)} (referred to hereafter as 6FDA-6FpDA), (b) poly({3,3′-(2,2,2-trifluoro-1-(trifluoromethyl)ethane-1,1-diyl)dianiline}-*alt*-{5,5′-(2,2,2-trifluoro-1-(trifluoromethyl)-ethane-1,1-diyl)bis(isobenzofuran-1,3-dione)}) (6FDA-6FmDA), and (c) poly((2,4,6-trimethyl-*m*-phenylenediamine)-*alt*-{5,5′-(2,2,2-trifluoro-1-(trifluoromethyl)ethane-1,1-diyl) bis(isobenzofuran-1,3-dione)}) (6FDA-DAM). Their chemical formulas are shown in Figure 1.

*Corresponding author.

Published on Web 02/05/2010

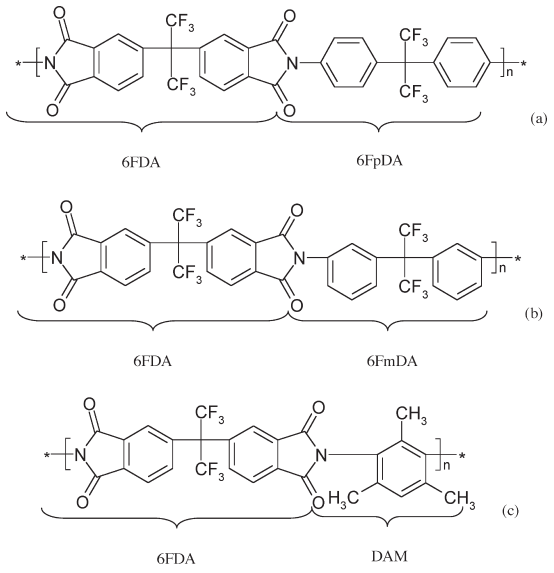

Figure 1. Chemical structures of (a) 6FDA−6FpDA, (b) 6FDA−6FmDA, and (c) 6FDA−DAM polyimides.

Note that 6FpDA is also sometimes referred to as BAAF,[39,60−63] 6FAP,[64,65] 4APF,[66] or BAHF,[67] that DAM can be called TrMPD[68−71] and 3MPDA,[55] and that 6FmDA corresponds to 3APF.[72] We have reported the results of a study of these three polyimides in the pure state in a recent paper,[73] and they are known to significantly vary in their CO_2 permeation properties.[40−45,48,50,52,59,62,63,74−76] It is worth noting that MD simulations of CO_2 transport in some of these systems have already been reported, but they were either restricted to very short simulation times[77,78] (60 ps) or used low-density approaches to create the models,[62,79] i.e., methods which are known to lead to a bias in the chain conformations.[80] Some of these simulations even used a simple spherical representation for CO_2. However, we are not aware of any full sorption isotherms and CO_2-induced volume swelling studied by MD simulations for these three fluorinated polyimides. As will be shown here, this requires a large number of simulation boxes with different CO_2 concentrations, which makes this work much more extensive than the aforementioned studies. An iterative technique[81] is then used to estimate the pressure of CO_2 that would have to be applied in order to obtain the imposed uptake. We note that the same iterative approach has recently been coupled to a novel particle deletion approach to estimating excess chemical potentials by Spyrionu et al. in order to determine the sorption of carbon dioxide in atactic polystyrene.[82] A related, but noniterative, approach has also been used to obtain the uptake curve of carbon dioxide in atactic polystyrene.[83] In this latter approach the pressure-dependent excess chemical potential in the condensed phase is estimated from the value obtained via test particle insertion at the reference pressure and a first-order Taylor series expansion involving an estimate of the partial molar volume from fluctuations in the volume at the reference pressure. The pressure in the corresponding gas phase is then obtained via a simulation in the pseudograd canonical ensemble.

In contrast to the situation regarding simulation studies, quite a few experimental investigations have been dedicated to study CO_2 transport and the subsequent plasticization effects in these three polyimides. Coleman et al.[40−42] investigated the effect of high-pressure CO_2 exposure on permeability in 6FDA-6FpDA and 6FDA-6FmDA. Costello and Koros[84] reported the temperature dependence of gas transport in the same polymers and gave dual-mode sorption parameters for CO_2. Singh-Ghosal and Koros[85] investigated mobility selectivity for 6FDA-6FpDA and 6FDA-6FmDA. Wang et al.[48] reported diffusivity, solubility and permeability for various gases in 6FDA-6FpDA. Fuhrman et al.[44] explained the thermal hysteresis of gas transport in 6FDA-6FpDA and 6FDA-6FmDA in terms of sub-T_g and T_g motions. Kim et al.[47,50−52] studied the effects of CO_2 exposure, physical aging, and chemical cross-linking on the gas separation abilities of both 6FDA-6FpDA and 6FDA-DAM. Recio et al.[43] reported the effect of the solvent used for the preparation of 6FDA-6FpDA membranes on the transport properties. Various other studies on CO_2 transport and plasticization effects also include these polymers or closely related structures.[38,45,55−58,60,63,64,74−76,86−95] Consequently, there is a lot of available experimental evidence to confront to the MD simulations.

Details of the MD simulations are given in section 2. They include the polymer models and the sample generation procedure, the choice of the CO_2 model, the addition of CO_2 into the preprepared polymer matrices, and its subsequent removal. The results obtained for the pure CO_2 vapor are given in section 3. In section 4, the results of the CO_2 uptake simulations into the polyimides are presented and discussed. Finally, the results of the CO_2 unloading simulations are presented and discussed in section 5.

2. Methods and Models

2.1. Iterative Method for Obtaining Sorption Isotherms. Our main aim in this work is to determine the full sorption isotherm of CO_2 in the model polyimides, i.e., the amount of CO_2 dissolved in the polymer as a function of the applied external pressure of carbon dioxide gas. In the laboratory this is a fairly routine experiment to perform by placing a polymer film in contact with the gas at a controlled pressure and measuring the mass change. Although this direct approach has also been mimicked in model systems,[96−101] it poses serious problems with respect to the creation of realistic membrane models and the time and length scales of the MD simulations. In effect, to have a sufficient amount of bulk polymer material at the center of the membrane implies a large membrane width (large system size), i.e., small surface area to volume ratio, but this inevitably leads to long simulation times as the attainment of equilibrium between the amount of gas in the gas phase and the amount of gas in the polymer phase is limited by the rate of diffusion of the gas in the polymer phase. In the case of CO_2 these diffusion rates are known from experiment to be too slow to reach equilibrium in a reasonable simulation time. An alternative approach is to first create models of the relaxed bulk polymers using standard 3D periodic boundary conditions. Such models have the advantage in that they do not contain any external surfaces, and as such, they are purely bulk models. The disadvantage of these fully 3D periodic models is that the number of gas molecules in the polymer system and the pressure become *independent* variables; i.e., we can insert as much gas as we want and set the pressure to any value. However, a fairly simple iterative technique[81] can be used to find the external pressure of the gas corresponding to the number of gas molecules in the system, and thus sorption isotherms can be calculated. The method is based on the fact that at equilibrium the chemical potential of the gas in the polymer phase, μ^p, and the gas in the gas phase, μ^g, are equal. Thus, for a polymer containing a fixed number of penetrant gas molecules, an NPT simulation, i.e., one in which the number of particles is fixed and pressure is controlled, is first made at some initial guess pressure, P_1. The resulting chemical potential of the gas in the polymer phase evaluated from this first simulation, $\mu^p(P_1)$, can then be used to obtain a second estimate of the pressure, P_2, from the (precalculated) chemical potential of the gas in the gas phase as a function of pressure, i.e., by finding the pressure in the gas phase where $\mu^g(P_2) = \mu^p(P_1)$. A second NPT simulation of the gas in the polymer phase is then carried out at an applied pressure of P_2. This in turn gives a

$\mu^p(P_2)$ which can again be used to obtain a third estimate $\mu^g(P_3) = \mu^p(P_2)$, and so on. In general, the method converges rapidly as dense polymer matrices are relatively incompressible so modest changes in pressure do not provoke much change in density and hence chemical potential.

In practice, chemical potentials are never actually calculated as certain simplifications can be made. In the case of a rigid gas molecule, as we will use for CO_2, the internal partition function is not dependent on the surrounding solvent so the equality of the chemical potential can be shown to be equivalent to the following condition[102,103]

$$\Delta\mu_{ex} = \mu^p_{ex} - \mu^g_{ex} = kT \ln \frac{\rho^g}{\rho^p} \tag{3}$$

which relates the difference in *excess* (with respect to the ideal gas) chemical potentials of the permeant in the two phases to their different densities in the two phases. A convenient statistical mechanical approximation for the excess chemical potential in the NPT ensemble is given by the following equation[104]

$$\mu_{ex} = -kT \ln \frac{\left\langle V \exp\left(\frac{-\Delta\Phi}{kT}\right)\right\rangle}{\langle V\rangle} \tag{4}$$

where $\Delta\Phi$ is the energy of interaction resulting from the *virtual* introduction of an extra test particle into an equilibrium distribution of the system in question and V is the volume of the system. Details of the specific test particle insertion method that has been used here and checks on its reliability are given below. In practice, then μ^g_{ex} and ρ^g have first to be calculated as a function of pressure for the pure gas system at the temperature required. μ^p_{ex} can then be calculated at a certain mass fraction of CO_2 in the polymer from a simulation conducted at the initial guess pressure, P_1. The quantities $\mu^p_{ex}(P_1) - \mu^g_{ex}(P)$ and $kT \ln[\rho^g(P)/\rho^p(P_1)]$ can then be plotted separately as a function of pressure, and the point of intersection of the two curves gives the second approximation, P_2. A further simulation of the gas in the polymer has then to be conducted at P_2, and the procedure iterated to convergence.

We note also that the relationship between the excess chemical potentials and the solubilities then follows directly from eq 3

$$\frac{\rho^g}{\rho^p} = \exp\left(\frac{\Delta\mu_{ex}}{kT}\right) = \frac{\exp\left(\frac{-\mu^g_{ex}}{kT}\right)}{\exp\left(\frac{-\mu^p_{ex}}{kT}\right)} = \frac{S^g}{S^p} \tag{5}$$

thus we can define a scale of (dimensionless) solubility using

$$S = \exp\left(-\frac{\mu_{ex}}{kT}\right) = \exp\left(\frac{kT \ln \frac{\left\langle V \exp\left(\frac{-\Delta\Phi}{kT}\right)\right\rangle}{\langle V\rangle}}{kT}\right) = \frac{\left\langle V \exp\left(\frac{-\Delta\Phi}{kT}\right)\right\rangle}{\langle V\rangle} \tag{6}$$

where a solubility of 1 corresponds to that of an ideal gas. In systems where volume fluctuations are relatively minor, e.g., dense polymers, the approximation $S \approx \langle \exp(-\Delta\Phi/kT)\rangle$ holds quite well.

2.2. MD Simulations. All MD simulations were performed using the scalar and parallel versions of the general purpose *gmq* program.[105] The parameters for the models of the polyimides were taken from the TRIPOS 5.2 force field.[106] The partial charges, q_i, on the atoms were calculated using *Gaussian 03*,[107] at the B3LYP/6-31G** level, on representative three- or five-fragment structures of the polyimides under study. For CO_2 the interaction parameters, including partial charges, were taken from optimized values reported by Zhang and Duan.[108] This is a rigid three-center model with a C−O bond length of 1.163 Å, a partial charge on the carbon atom of $q_C = 0.5888e$ (and neutralizing charges on the oxygens of $q_O = -q_C/2$), and Lennard-Jones 12−6 interaction sites situated at the carbon and oxygen centers with $\sigma_{C-C} = 2.7918$ Å, $\varepsilon_{C-C}/k_B = 28.845$ K, $\sigma_{O-O} = 3.0$ Å, and $\varepsilon_{O-O}/k_B = 82.656$ K.

The equations of motion were integrated using a 1 fs integration time step. The SHAKE algorithm[109] was used to constrain all bond lengths. In addition to simple bond constraints, a special vector constraint was used to keep the bond angle of CO_2 (O−C−O) fixed at 180°.[110] The CO_2 molecule is thus completely rigid and just has five degrees of freedom: three translations and two rotations. We think that it is important to point out that, without the bond angle constraint, the (flexible angle) model would acquire two extra degrees of freedom: an angle bend *and* a rotation around the long O−C−O axis. This latter degree of freedom has a vanishingly small moment of inertia associated with it and thus couples very poorly to the other degrees of freedom. This leads almost inevitably to a nonequipartition of kinetic energy in a classical MD simulation. Although this point has been known about for over 25 years, it has tended to be forgotten in recent times.[111−113]

The loose-coupling procedure was used to maintain the temperature and pressure close to the required values.[114,115] A loose coupling relaxation time of 0.1 ps was used for the temperature and 5 ps for the pressure. The Ewald summation method[116] was used to calculate the electrostatic interactions. In all cases the three parameters controlling the convergence of the Ewald sum: R_c, the real space cutoff, K_{max}, the maximum integer defining the range of the reciprocal space sum, and α, the separation parameter, were optimized in order to give an agreement of less than 1 bar between the direct and indirect calculations of the Fourier space contribution to the pressure.[105,117]

The Lennard-Jones 12−6 form was used to represent all the van der Waals interactions with the Lorentz−Berthelot combining rule for unlike atom types: $\sigma_{AB} = (\sigma_{AA} + \sigma_{BB})/2$ and $\varepsilon_{AB} = (\varepsilon_{AA}\varepsilon_{BB})^{1/2}$. The same real space truncation radius was used as optimized for the real space part of the Ewald sum. In all cases R_c exceeded 10 Å. Standard long-range corrections were made systematically to the Lennard-Jones 12−6 potential contributions to the energy and pressure by assuming that the radial distribution functions were unity for distances greater than R_c.

2.3. Pure Polyimides. Most details of the preparation of the relaxed models of the pure polymers have already been reported elsewhere[73] so only a brief outline will be presented here. The hybrid pivot Monte Carlo−molecular dynamics (PMC-MD) single-chain sampling technique was used to generate the initial conformations of the different types of polymer chains at temperatures just above their respective glass transition (T_g), i.e., 700 K for 6FDA-6FpDA and 6FDA-DAM and 600 K for 6FDA-6FmDA. Each chain contained 50 repeat units. Two different sizes of polymer matrices, 3-chain (~10 000 atoms) and 6-chain (~20 000 atoms), were prepared for each type of polymer by inserting the required number of independently generated chains into a periodic MD box of a size corresponding to the experimental density at 298 K. Excluded volume was then introduced gradually. The simulation boxes with the complete potential switched on were then allowed to relax under NVT (constant number of atoms, constant volume, and controlled temperature) conditions for 500 ps and then cooled down to 298 K at the rate of 1 K/ps. After a short NVT relaxation at 298 K the simulation boxes were allowed to relax under NPT (constant number of atoms, controlled pressure, and

temperature) conditions for 3 ns. These relaxed samples at 298 K were the subject of a precedent article.[73] The relaxed densities of the three model polymers were in good agreement with the available experimental data. Their X-ray diffractograms, fractional free volumes, and Hildebrand solubility parameters were also calculated and validated against available experimental results. In addition, the intermolecular and intramolecular interactions and void space distributions were analyzed.

In general, experimental sorption studies of carbon dioxide in polymers are performed above the critical temperature of CO_2 (~304 K). For this reason the configurations at the end of the MD simulations at 298 K were first heated to 308 K, at the rate of 1 K/ps, and then the simulations were continued under NPT conditions for a further 4 ns. The resulting relaxed samples at 308 K were then used as the starting points for all subsequent sorption studies.

2.4. Pure Carbon Dioxide. The optimized all-atom potential parameters reported by Zhang and Duan[108] were used to simulate CO_2. This potential is reported to reproduce the liquid−vapor coexistence properties of carbon dioxide over a wide range of temperatures and pressures and predicts a critical temperature in good agreement with the experimental value of 304 K. As explained above, in this work it is required to know for this model of CO_2 the equilibrium pressure, density, and excess chemical potential of the vapor along the 308 K isotherm. This is effectively the vapor phase which we consider to be in equilibrium with the gas sorbed in the polymers. MD simulations on systems of 512 molecules were carried out for 4 ns under NVT conditions using volumes determined by interpolation from the experimental data of Span and Wagner.[118] The last 3 ns of these simulations was used to obtain the corresponding average properties including the pressure.

2.5. Carbon Dioxide Uptake into Polyimides. The calculation of the sorption isotherms were started from the pure polyimide matrices at 308 K, and as a first guess, the equilibrium pressures were set to 1 bar. Random insertion of CO_2 molecules into systems containing the polyimides can lead to large overlaps and even ring spearings. In order to avoid this, equilibrated dense systems of CO_2, at densities of ~1000 kg m^{-3}, were prepared in boxes of the same size as the polyimide-containing simulation boxes; these could be either pure polyimide systems or systems already containing both polyimide and CO_2. The CO_2 and the polyimide-containing simulation boxes were superimposed, and the desired numbers of CO_2 molecules were inserted into the polyimide-containing systems from those that overlapped the least. After the insertion of CO_2, a few steps of energy minimization was required to remove the remaining small overlaps. The systems were then relaxed under NVT conditions for 50 ps before being switched to NPT conditions for the production run. Most simulations were initially run for 4000 ps under NPT conditions, at the initial guess pressure of 1 bar, of which the final 3000 ps was used to calculate the averages including the excess chemical potential. Root-mean-square displacements of the carbon dioxide molecules were systematically monitored, and these were typically in excess of 20 Å in a period of 4 ns. This is more than sufficient to decorrelate their positions with respect to the initial insertions and thus minimize any artifacts due to the choice of insertion procedure.

An estimation of the pressure of CO_2 vapor that has to be applied to obtain the imposed uptake was then obtained using the technique described in section 2.1. If this pressure exceeded 10 bar, i.e., sufficiently different in MD terms from the initial pressure, then this pressure was applied in a second NPT simulation of 3 ns, starting from the end of the first production run. The average excess chemical potential from this second run was then used to check for convergence of the iterative method. Within errors the left- and right-hand sides of eq 3 were the same for all these systems after just one iteration. In effect, the first estimate of the equilibrium vapor pressure obtained from the simulations at 1 bar was already quite reasonable.

To mimick the experimental approach, and to avoid the necessity of preswelling the polyimide containing systems, CO_2 loading was carried out in a progressive way. Pure polyimide samples were initially loaded with an amount of CO_2 corresponding to ~1% of the mass of the pure polyimide systems; in the ~10 000-atom systems, this corresponds to 25 molecules in the case of 6FDA-6FpDA and 6FDA-6FmDA and 19 molecules in the case of 6FDA-DAM. To obtain higher loadings, copies of configurations at the preceding loading were made after 500 ps of the corresponding NPT simulation, a time sufficient to allow for most of the volume swelling to occur. These copies were then used to start off simulations at higher loadings by adding a further ~2 mass % of CO_2, i.e., 50 molecules in the case of 6FDA-6FpDA and 6FDA-6FmDA and 38 molecules in the case of 6FDA-DAM for the ~10 000-atom systems. This procedure of adding 2 mass % was continued up until 25% of CO_2 had been added. Note that the simulations at 9% and 13% of CO_2 were not systematically extended for all systems beyond the 500 ps necessary to relax the systems for the next addition of 2%. Given the relatively small changes in pressure in this region the simulations at 9% and 13% were considered superfluous. Results for each type of polyimide were averaged over three independent systems.

2.6. Carbon Dioxide Unloading from Polyimides. As hysteresis has been seen when performing desorption experiments after conditioning samples,[41,42,44,45,84] it was considered interesting to obtain the unloading curves from the model systems. In real experiments the applied vapor pressure of CO_2 is the controlled variable, and data exist for desorption curves starting from systems held at 60 bar.[41] For the 6FDA-DAM systems further loading, in 2% increments, up to ~31% was first required so as to attain a pressure of ~60 bar. The number of CO_2 molecules in the samples was then adjusted, on the basis of the sorption curves, in order to have an amount that corresponded to a pressure of ~60 bar. In terms of the mass of the pure polyimide systems, this was about 24.3%, 23.1%, and 31.1% of CO_2 for 6FDA-6FpDA, 6FDA-6FmDA, and 6FDA-DAM, respectively. As for the insertions, removal of CO_2 was also done in a progresive stepwise procedure. As for the loading curves, copies of the configurations obtained after 500 ps of NPT simulation were taken, a further 2% of the CO_2 was removed, and the resulting configurations were used as the initial configuration at the lower amount. The removal was continued all the way back down to the pure polymer matrices. Most of these simulations were carried out for 4 ns with averages obtained from the last 3 ns. The pressure in these desorption simulations was set to 1 bar so as to have direct comparisons with the uptake simulations. Given the results for the uptake curve, the corresponding equilibrium vapor pressures of the gas for the desorption were mostly obtained from the first estimate. Checks made on some systems again confirmed that this was in agreement with the converged values. The results presented are for just one sample for each type of polyimide.

2.7. Test Particle Insertion Using Excluded Volume Map Sampling. In this work a test particle insertion (TPI) method employing a variant of the excluded volume map sampling (EVMS) approach[119,120] was used to calculate the excess chemical potentials of CO_2 in the pure polymer, polymer plus CO_2, and pure CO_2 systems. In the EVMS technique a large amount of the occupied space is pre-eliminated before particle insertions are attempted in order to improve the efficiency compared to purely random insertions. The details of this approach have been documented elsewhere;[105] hence, only a short description is presented here.

In the method, the MD box is first divided up into a number of subcells on the basis of an input subcell width, d_{grid}. As the MD box is not necessarily cubic and the number of subcells in each direction has to be an integer, the subcells are constructed internally on the basis of this subcell width. In a second step, each atom in the system is visited and all subcells that fall

entirely within a critical radius, w_{cut}, of the atom are mapped out; i.e., w_{cut} represents the "excluded" volume of an atom. Particle insertions are then made by randomly choosing one of the "mapped-in" subcells and then randomly placing and orientating a probe molecule within the chosen subcell. In this way occupied space can be pre-eliminated while preserving the advantages of a Monte Carlo sampling of space. The actual amount of space mapped out depends on the w_{cut} and d_{grid} parameters. A finer grid will pre-eliminate more space at the cost of a larger overhead in terms of memory and CPU time required to set up the map for each configuration. As the EVMS method performs a biased sampling of the space the results have to be corrected for the bias. This is done by simply assuming that $\exp(-\Delta\Phi/kT)$ in the mapped-out cells is zero in which case true averages are approximated by multiplying by the ratio of the number of mapped-in cells to the total number of cells.

The difficulty with this EVMS method is knowing *a priori* what an appropriate value of w_{cut} should be for a particular system. For this reason different values of w_{cut} have to be first tested in a mode where trial insertions are made into the "mapped-out" cells, i.e., those nominally occupied by the particles present in the system. If the value of w_{cut} is appropriate, then insertions into mapped-out cells should always give large positive (unfavorable) energy changes. However, should a favorable insertion be made ($\Delta\Phi \leq 0$), then the test has failed and a smaller value of w_{cut} has to be tried. In this way w_{cut} can be optimized, so as to pre-eliminate as much space as possible, without allowing favorable insertions in the mapped-out subcells. In this work many tests were made and appropriate values were found to be $w_{cut} = 2$ Å and $d_{grid} = 0.5$ Å for the case of CO_2 in the polyimides.

At best an EVMS method can improve the efficiency of a particle insertion approach by a factor of the total volume divided by the mapped-in volume, e.g., a factor of 20 if 95% of the space is considered occupied; in practice, the overheads associated with pre-eliminating 95% of the space are not negligible. Claims to factors of improvement of EVMS over conventional particle insertion greater than 20[120] should probably be treated with some skepticism.

In the case of a charge neutral probe molecule, like carbon dioxide, there is a subtle point to consider concerning the calculation of the energy difference. In principle, the energy difference we require is just the interaction of the test particle with the real particles already present. If the Ewald summation is used to obtain the Coulombic part of this energy difference, using $\Delta\Phi_c = \Phi_c(N+1) - \Phi_c(N)$, there is a problem in that intrinsically the Ewald sum contains contributions from probe molecule interactions with *images* of itself and interactions of real particles with *images* of the probe molecule. The interaction energy of the probe with images of itself are removed in our code by performing the Ewald sum on the probe molecule alone in the MD box. However, this does not remove interactions of real particles with images of the probe so the energy difference does not strictly correspond to that of the interaction of one probe with an infinite array of real particles. As the probe molecules are relatively small in size and charge neutral, this term is probably not of any importance in practice.

Although the EVMS method has been verified against the standard random insertion approach in the case of the Lennard-Jones fluid, it was considered prudent to first make a check in the case of carbon dioxide, in particular given the significant partial charges on the atoms of these molecules. The system chosen to make the test was pure liquid CO_2 at 290 K at a density of 804.722 kg m^{-3}, i.e., close to the liquid−vapor coexistence curve. This represents a reasonably stiff test of the EVMS method as although a significant amount of CO_2 can be absorbed by the polymers in question at 308 K, it is unlikely that the local density of CO_2 exceeds that of the pure liquid at 290 K. A system of 512 molecules of CO_2 was, thus, equilibrated in a cubic MD box at a density of 804.722 kg m^{-3} at 290 K.

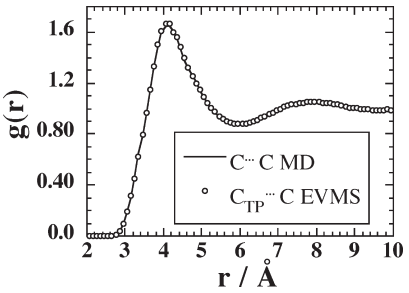

Figure 2. Intermolecular radial distribution functions, $g(r)$, obtained for actual C···C interactions from stored configurations (solid line) from the MD simulation of pure liquid CO_2 at 290 K compared to those obtained by Boltzmann factor weighting test particle−actual particle interactions (C_{TP}···C) during the EVMS particle insertion tests (circles) on the same set of configurations.

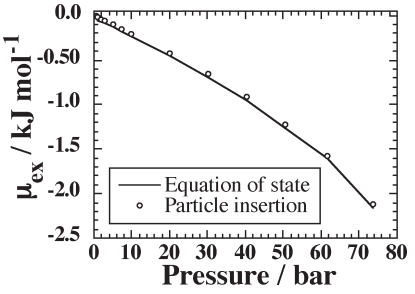

Figure 3. Excess chemical potential of carbon dioxide in the pure vapor phase at 308 K. Results for the direct evaluation of the excess chemical potential using the EVMS test particle insertion method (circles) are compared to the results obtained using the equation of state approximation given in eq 7 (line).

Configurations from an NVT production run of 300 ps were stored every 1 ps, and these were then used to make the EVMS particle insertion tests. For the case of pure carbon dioxide at 290 K it was found that a $w_{cut} = 2.4$ Å could be used. A value of $d_{grid} = 0.1$ Å was also used, and this led to about 77% of the space being mapped out. With a required density of test particle insertions of 10 $Å^{-3}$ this resulted in just over 100 000 test insertions per configuration. The validation of the EVMS method was first made by comparing the Boltzmann factor weighted radial distribution functions accumulated during the test particle insertions to those obtained from the production simulation itself. Figure 2 shows the comparison in the case of carbon−carbon interactions. Although not shown, similar excellent agreement was obtained for the carbon−oxygen and oxygen−oxygen interactions.

As a confirmation of the results for the radial distribution functions, the Boltzmann-weighted average insertion energy of the CO_2 test particle, $\langle\Delta\Phi \exp(-\Delta\Phi/kT)\rangle/\langle\exp(-\Delta\Phi/kT)\rangle = -17.06 \pm 0.03$ kJ mol^{-1} (of CO_2), compared well to that inferred from the average total potential intermolecular energy in the MD simulation, -17.02 ± 0.02 kJ mol^{-1} (of CO_2). It is thus reasonable to conclude that the EVMS test particle insertion technique is reliable for CO_2.

3. Pure Carbon Dioxide Vapor at 308 K

From the MD simulations on systems of pure CO_2 in the vapor phase, the excess chemical potential was extracted using the EVMS test particle insertion method from the configurations stored over the last 3 ns of the corresponding simulations. The results obtained are plotted as a function of the average pressure, obtained from the same simulations, in Figure 3. The excess chemical potentials calculated directly from test particle insertions were compared with the values obtained from the following

Table 1. Average Results of the Sorption Isotherm MD Simulations at 308 K on 6FDA-6FpDA[a]

~% CO_2	no. of CO_2	true concn $V_g^{STP}(P)/V(P)$	nominal concn $V_g^{STP}(P)/V_0$	P/bar	true solubility $C(P)/P$	nominal solubility $C_0(P)/P$	TPI solubility
0	0	0.00	0.00	0			124 ± 4
1	25	7.52 ± 0.02	7.51 ± 0.02	0.08 ± 0.01	98 ± 8	98 ± 8	102 ± 2
3	76	22.8 ± 0.1	22.8 ± 0.04	0.23 ± 0.06	117 ± 37	117 ± 37	77 ± 2
5	127	38.1 ± 0.1	38.11 ± 0.06	0.68 ± 0.03	56 ± 3	56 ± 3	56 ± 3
7	177	52.7 ± 0.2	53.11 ± 0.09	1.5 ± 0.1	37 ± 2	37 ± 2	37 ± 2
11	278	81.5 ± 0.3	83.5 ± 0.2	5.2 ± 1.0	17 ± 4	18 ± 4	17 ± 4
15	380	108.4 ± 0.5	114.1 ± 0.2	12 ± 2	9.7 ± 1.6	10.2 ± 1.7	9.4 ± 1.9
17	430	120.5 ± 0.3	129 ± 0.2	29 ± 2	4.2 ± 0.2	4.5 ± 0.3	4.2 ± 0.2
19	481	132 ± 1	144 ± 0.3	38 ± 5	3.6 ± 0.4	3.9 ± 0.4	3.5 ± 0.4
21	531	143 ± 1	159 ± 0.3	41 ± 14	4.3 ± 1.2	4.8 ± 1.3	4.2 ± 1.2
23	582	154 ± 1	175 ± 0.4	41 ± 9	4.1 ± 0.9	4.7 ± 1.1	4.2 ± 1.1
25	633	164 ± 1	190 ± 0.4	76 ± 15	2.3 ± 0.4	2.7 ± 0.5	2.2 ± 0.4

[a] The averages are taken from three independent systems. The approximate mass percentages of CO_2 are given as obtained from the actual number of molecules inserted into the polymers. The corresponding true and nominal concentrations of gas in the polymer are shown in units of cm^3 (STP) cm^{-3} of polymer (true or pure polymer volume). The pressure given is that estimated to be the equilibrium external vapour pressure of CO_2 which would have to be applied to give the imposed concentrations of CO_2 in the polymer. The true and nominal solubility coefficients are given as well as the solubility coefficient estimated from the EVMS test particle insertion analysis (eq 10 or 11) in units of cm^3 (STP) cm^{-3} bar^{-1}. Error bars are the standard errors over the three independent systems.

Table 2. As Table 1 for 6FDA-6FmDA

~% CO_2	no. of CO_2	true concn $V_g^{STP}(P)/V(P)$	nominal concn $V_g^{STP}(P)/V_0$	P/bar	true solubility $C(P)/P$	nominal solubility $C_0(P)/P$	TPI solubility
0	0	0.00	0.00	0			116 ± 10
1	25	7.55 ± 0.01	7.59 ± 0.02	0.08 ± 0.01	100 ± 18	100 ± 18	101 ± 11
3	76	22.9 ± 0.01	23.1 ± 0.1	0.21 ± 0.04	120 ± 30	121 ± 30	82 ± 5
5	127	38.2 ± 0.1	38.5 ± 0.1	0.69 ± 0.06	56 ± 5	57 ± 5	54 ± 4
7	177	52.9 ± 0.2	53.7 ± 0.1	1.39 ± 0.15	39 ± 4	39 ± 4	39 ± 4
11	278	81.4 ± 0.2	84.4 ± 0.2	4.9 ± 1.1	18.7 ± 5.1	19.4 ± 5.2	19 ± 5
15	380	107.9 ± 0.3	115.3 ± 0.2	11.4 ± 3.2	10.8 ± 2.4	11.6 ± 2.6	11 ± 2
17	430	120.1 ± 0.3	130.5 ± 0.3	16.4 ± 3.1	8.0 ± 1.8	8.7 ± 2	8.2 ± 1.8
19	481	132.0 ± 0.5	145.9 ± 0.3	32 ± 7.5	4.7 ± 1.3	5.2 ± 1.5	4.7 ± 1.0
21	531	143 ± 1	161.1 ± 0.3	58 ± 5.5	2.5 ± 0.3	2.9 ± 0.3	2.6 ± 0.3
23	582	155 ± 1	176.6 ± 0.4	59 ± 2.5	2.6 ± 0.1	3.0 ± 0.1	2.5 ± 0.1
25	633	165 ± 1	192.0 ± 0.4	100 ± 0.6	1.65 ± 0.01	1.92 ± 0.01	1.7 ± 0.2

Table 3. As Table 1 for 6FDA-DAM

~% CO_2	no. of CO_2	true concn $V_g^{STP}(P)/V(P)$	nominal concn $V_g^{STP}(P)/V_0$	P/bar	true solubility $C(P)/P$	nominal solubility $C_0(P)/P$	TPI solubility
0	0	0.00	0.00	0			121 ± 9
1	19	6.71 ± 0.02	6.70 ± 0.03	0.07 ± 0.01	92 ± 9	92 ± 9	106 ± 10
3	57	20.07 ± 0.06	19.74 ± 0.08	0.20 ± 0.05	124 ± 43	122 ± 43	81 ± 3
5	95	33.43 ± 0.09	33.5 ± 0.1	0.54 ± 0.01	62 ± 1	62 ± 1	64 ± 4
7	133	46.6 ± 0.1	46.5 ± 0.2	0.92 ± 0.07	51 ± 4	51 ± 4	49 ± 3
11	209	72.4 ± 0.2	73.7 ± 0.3	3.0 ± 0.4	25 ± 4	25 ± 3	25 ± 3
15	285	96.6 ± 0.3	100.5 ± 0.4	10.4 ± 2.4	10.1 ± 1.9	11 ± 2	10.2 ± 1.6
17	323	107.7 ± 0.3	113.9 ± 0.4	11.8 ± 1.1	9.3 ± 1.0	9.8 ± 1.0	9.5 ± 0.7
19	361	118.3 ± 0.5	127.3 ± 0.5	13.8 ± 2.6	9.2 ± 1.6	9.9 ± 1.8	9.4 ± 1.4
21	399	128.8 ± 0.4	140.7 ± 0.6	28.9 ± 4.9	4.7 ± 0.7	5.2 ± 0.8	6.7 ± 1.2
23	437	139.3 ± 0.2	154.1 ± 0.6	26.9 ± 3.1	5.3 ± 0.7	5.9 ± 0.7	5.1 ± 0.1
25	475	149.1 ± 0.3	167.4 ± 0.7	40 ± 5	3.9 ± 0.6	4.3 ± 0.7	3.6 ± 0.4
27	513	158.1 ± 0.5	180.8 ± 0.7	46 ± 3	3.5 ± 0.2	4.0 ± 0.3	3.6 ± 0.2
29	551	166.0 ± 0.3	194.2 ± 0.8	41 ± 5	4.2 ± 0.6	4.9 ± 0.7	4.0 ± 0.6
31	589	175.4 ± 0.5	207.6 ± 0.8	57 ± 11	3.3 ± 0.5	3.9 ± 0.6	3.1 ± 0.3

equation, based on a knowledge of the equation of state (see Appendix).

$$\mu_{ex} = -kT \ln\left[\frac{\rho(P',T)}{\rho^{ig}(P',T)}\right] + \frac{1}{N}\int_{P_{low}}^{P'} (V(P,T) - V^{ig}(P,T))\, dp \quad (7)$$

where ρ^{ig} and V^{ig} are the density and volume of the corresponding ideal gas. In eq 7, it is assumed that there exists a sufficiently low pressure, P_{low}, that the gas behaves in an ideal manner, and thus the difference in the actual and ideal volumes disappears in the integral. For the model of CO_2 used here, even at the lowest pressures simulated, there existed some deviations from ideality. As volume is (roughly) inversely proportional to pressure the difference in volume at low pressures rapidly become very significant, thus rendering the use of eq 7 subject to a certain degree of error. This problem manifests itself in an offset of the curve at low pressures which is obviously present at all higher pressures. Nevertheless, the comparison shown in Figure 3 is reasonably consistent. For all subsequent calculations involving the excess chemical potential of the vapor phase we stress that the values obtained directly from the test particle insertion approach will be used.

4. Carbon Dioxide Uptake into Polyimides

In this section we present and discuss the results of the simulations described in section 2.5 in which carbon dioxide is progressively loaded into the three types of polyimides, and the equilibrium pressure of CO_2 corresponding to the imposed quantity of CO_2 is obtained through the iterative technique

described in section 2.1. All results in this section are averaged over three independent systems for each of the three polyimides.

4.1. Sorption Isotherms. The results obtained using the iterative method described above for the equilibrium external gas pressure corresponding to the numbers of CO_2 molecules inserted into the different polymers are shown in Tables 1, 2, and 3. The true concentrations of gas in the polymer, $C(P)$, have been expressed as the ratio of the "volume" of gas absorbed by a certain volume of polymer

$$C(P) = \frac{V_p^{STP}(P)}{V(P)} = \frac{n_p(P)k_B T^{STP}}{V(P)P^{STP}} \tag{8}$$

The volume V_p^{STP} is the volume that the $n_p(P)$ molecules of gas absorbed in the polymer would occupy if the gas were ideal and at the standard temperature and pressure (T^{STP} = 273.15 K; P^{STP} = 1.013 25 bar) conditions, and $V(P)$ is the true volume of the polymer. However, in order to compare with the usual experimental practice, the nominal concentrations of the gas in the polymer at the different pressures, $C_0(P)$, have also been calculated using the following definition

$$C_0(P) = \frac{V_p^{STP}(P)}{V_0} = \frac{n_p(P)k_B T^{STP}}{V_0 P^{STP}} \tag{9}$$

where V_0 is the corresponding volume of the *pure* polymer, i.e., before any gas has been absorbed. In reality, the true volume of the polymer, $V(P)$, changes as a function of the applied gas pressure as it absorbs more and more gas, but most experiments do not measure simultaneously the volume of the polymer and the gas uptake. For completeness, both the true and nominal concentrations are given in the tables. From the converged value of the pressure, P, the corresponding true and nominal solubility coefficients can be defined as, $S(P) = C(P)/P$ and $S_0(P) = C_0(P)/P$, respectively. These values are also given in the tables. Finally, to check the consistency of the iterative approach, the solubility coefficient as obtained from the test particle insertion method has also been calculated, $S^{TPI}(P)$. Using eqs 5 and 8, we can write

$$\frac{C(P)}{P} = \frac{n_p(P)k_B T^{STP}}{V(P)PP^{STP}} = \frac{\rho^p(P)k_B T^{STP}}{PP^{STP}}$$

$$= \frac{S^p(P)\rho^g(P)k_B T^{STP}}{S^g(P)PP^{STP}} \equiv S^{TPI}(P) \tag{10}$$

thus eliminating the explicit appearance of the concentration of gas in the polymer from the expression for the solubility coefficient. In the limit that P tends to zero, the ideal gas law can be invoked in which case the number density in the gas phase can be replaced by $\rho^g(P) = P/k_B T$ and the solubility in the gas phase becomes unity, $S^g(P) = 1$, so eq 10 becomes

$$\lim_{P\to 0} S^{TPI}(P) = \frac{S^p(P)\dfrac{P}{k_B T}k_B T^{STP}}{S^g(P)PP^{STP}} = \frac{S^p(P)T^{STP}}{TP^{STP}} \tag{11}$$

TPI-derived estimations of the solubility coefficients are also given in the tables. For all nonzero pressures eq 10 was used, and estimates at zero pressure were obtained from eq 11.

The results shown in Tables 1−3 demonstrate the robustness of the iterative technique. In general, the equilibrium pressure is found to increase smoothly with loading, as one would expect. Slight variations in the average trend result from statistical noise. The reduction in the difference in the slopes of the quantities $\mu_{ex}^p(P_1) - \mu_{ex}^g(P)$ and $kT \ln[\rho^g(P)/\rho^p(P_1)]$ at the higher pressures also leads to less precision on the point of intersection. At the lowest imposed concentrations of gas in the polymers, the equilibrium pressures were below the ~0.5 bar lower limit of the explicit simulations of the pure gas. In these cases linear interpolations have been used to obtain the excess chemical potential and the density of the gas phase on the basis that the excess chemical potential and the density of the gas phase both tend to zero as the pressure tends to zero.

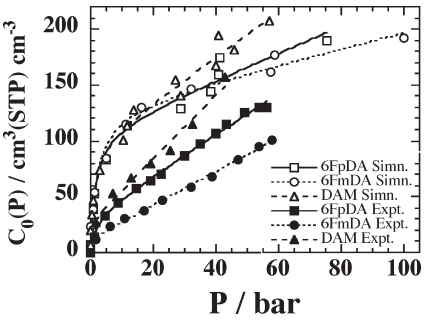

Figure 4. Comparison of CO_2 sorption isotherms of 6FDA-6FpDA, 6FDA-6FmDA, and 6FDA-DAM at 308 K, as obtained from the simulations reported here and experimental data taken from the papers of Coleman and Koros[41] (6FDA-6FpDA and 6FDA-6FmDA) and Wind et al.[122] (6FDA-DAM). The nominal concentrations (eq 9) are plotted as a function of the partial pressure of carbon dioxide. Smooth lines through the data are nonlinear least-squares regression fits to the concentration form of the dual mode sorption model (eq 12). For clarity, error bars on the pressure in the simulation data have been omitted.

Figure 4 shows the average sorption isotherms of the three polyimides in terms of the nominal concentration, $C_0(P)$. The smooth curves plotted through the data are nonlinear least-squares regression fits to the dual mode sorption (DMS) model

$$C_0(P) = k_D P + C_H' \frac{bP}{1+bP} \Rightarrow S_0(P) = \frac{C_0(P)}{P}$$

$$= k_D + C_H' \frac{b}{1+bP} \tag{12}$$

The DMS model is still a popular way of fitting such data even though careful analyses of experimental data obtained over increasing pressure ranges show clearly that the "constant" parameters (k_D, C_H', and b) are not at all constant but vary systematically with the pressure range used.[121] It should also be noted that recent molecular simulations have shown that the penetrant uptake curves can be fitted using the form of eq 12 without any evidence of two different populations of sorbed species at the molecular level.[101]

Also shown in Figure 4 are some corresponding experimental data taken from the literature. In general, the experimental data obtained for the greatest range of pressure has been chosen to make the comparison. In the case of 6FDA-6FpDA this was the data of Coleman and Koros[41] which was found to be in good agreement with the data of Wang et al.[48] and Hibshman et al.[59] For 6FDA-6FmDA, the data were again taken from the work of Coleman and Koros[41] which was again consistent with later work published by the same authors.[42] For 6FDA-DAM, the only experimental data that were found at a range of pressures were that of Wind et al.[122] Hölck et al. have performed a single sorption measurement of CO_2 in 6FDA-DAM at a pressure of 10 bar and at

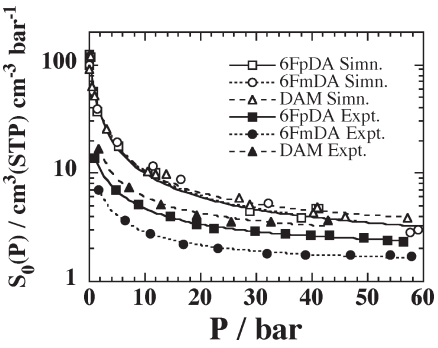

Figure 5. As Figure 4 for the nominal solubilities. Note the logarithmic scale on the *y*-axis. Smooth lines through the data are nonlinear least-squares regression to the solubility form of the dual mode sorption model (eq 12); we note in passing that the best fit DMS parameters depend on whether solubility or concentration curves are fitted. For clarity, error bars on the pressure in the simulation data have again been omitted.

308 K.[79] Their reported nominal concentration of 81.4 cm^3 (STP) cm^{-3} at 10 bar lies about midway between that of Wind et al.[122] and our simulation result.

In the low pressure range, there is a marked contrast in the behavior of the concentration with pressure between simulation and experiment. The simulation data all show a very rapid and very similar increase in concentration below 10 bar, whereas the experimental data increase at a much slower rate and differences between the polymers are evident at much lower pressures. At higher pressures, the faster rate of increase of the concentration of CO_2 in 6FDA-DAM is clear to see in the simulation data although a difference between 6FDA-6FpDA and 6FDA-6FmDA is not evident until above 60 bar. The models thus predict the same trends as experiment, but the two isomers behave in a more similar way than actually found.

The notably more rapid increase in concentration with pressure implies higher solubilities in the models. This is apparent in Figure 5 where the corresponding nominal solubilities have been plotted.

The limiting zero pressure solubilities in the model systems are all high and quite close (120 ± 10 cm^3 (STP) cm^{-3} bar^{-1}) compared to the experimental results: ~21 for 6FDA-6FpDA, ~14 for 6FDA-6FmDA, and ~36 for 6FDA-DAM, as estimated from the best fit DMS parameters ($S_0(P\rightarrow 0) = k_D + C'_H b$). The discrepancy between simulated and experimental solubility values in the infinite dilution limit is a problem which has been known for a long time,[123] and we will come back to some possible explanations. Following this low-pressure range, model solubilities drop very sharply in the 0−20 bar pressure range and approach progressively the experimental values. For 6FDA-DAM, the agreement is especially good with both model and experiment having limiting high-pressure nominal solubilities of ~4 cm^3 (STP) cm^{-3} bar^{-1}. In the cases of 6FDA-6FpDA and 6FDA-6FmDA, the model solubilities remain higher but only by a factor of about 2, which can also be considered as satisfactory. It would thus seem that the models predict better the limiting (Henry's law) sorption but rather overestimate the initial (Langmuir-like) uptake. Indeed, simulation works often quote solubilities at pressures away from the infinite-dilution limit[124] where experimental data exist. In the rest of this section, we investigate and speculate on some of the reasons that may lie behind these discrepancies in the infinite dilution limit.

First of all, as noted above, it is not unusual for empirical force field based molecular simulations to overestimate solubilities of gases in polymers or, more specifically, of CO_2 in glassy polymers in the infinite dilution limit.[124] Heuchel et al. have published estimates of limiting low-pressure solubilities of a single interaction center model of CO_2 in a number of polyimides, including 6FDA-6FpDA (106 ± 18 cm^3 (STP) cm^{-3} bar^{-1}) and 6FDA-DAM (68 ± 5 cm^3 (STP) cm^{-3} bar^{-1}).[62] Their results are consistently higher than the quoted (partial pressure of CO_2 unspecified) experimental values. Unfortunately, it is unclear how the cross-interactions between the single Lennard-Jones 12−6 site model of CO_2 and atoms in the polyimides (COMPASS force field, i.e., with Lennard-Jones 9−6 potentials) are calculated. Nevertheless, to assess the effect of changing from an all-atom model of CO_2 with partial charges to a single neutral spherical representation, the solubilities of a single Lennard-Jones site model, with the parameters given by Heuchel et al. (σ = 4 Å, ε/k_B = 226.23 K),[62] in our pure PI systems have been calculated using the TPI method. The resulting average solubility coefficients were 450 ± 40, 382 ± 13, and 354 ± 22 cm^3 (STP) cm^{-3} bar^{-1} for 6FDA-6FpDA, 6FDA-6FmDA, and 6FDA-DAM, respectively. The considerably higher solubilities obtained suggest that the spherical representation of CO_2 is poorly adapted for such studies. Further tests using the single LJ site potential parameters optimized for supercritical CO_2 of Iwai et al.[125] (σ = 3.72 Å, ε/k_B = 236.1 K) gave the resulting average solubility coefficients of 253 ± 7, 220 ± 5, and 198 ± 6 cm^3 (STP) cm^{-3} bar^{-1} for 6FDA-6FpDA, 6FDA-6FmDA, and 6FDA-DAM, respectively. Again these are still higher than the three-site model used here.

The concern about the parametrization of the van der Waals part of the cross interactions, in particular in this case between the gas and the polymer, should not be underestimated either. In general, the force fields for the pure systems, polymer or gas, are developed independently with little or no attention paid to optimizing the gas−polymer interactions. Empirical mixing rules, such as the Lorentz−Berthelot ones used here, are known to have their limitations even for mixtures of rare gases.[126] Previous molecular level simulations of helium in polyimides have investigated the effect of the cross-interactions by comparing different combining rules and concluded that this can influence solubilities and diffusion.[98] In order to estimate the degree of such effects in the case of carbon dioxide, the TPI calculations on the pure polymer systems have been repeated using the Waldman−Hagler[126] combination rules: $\sigma_{AB} = [(\sigma_{AA}^6 + \sigma_{BB}^6)/2]^{1/6}$ and $\varepsilon_{AB} = (\varepsilon_{AA}\varepsilon_{BB})^{1/2}[2\sigma_{AA}^3\sigma_{BB}^3/(\sigma_{AA}^6 + \sigma_{BB}^6)]$, for just the CO_2−polymer interactions. The resulting TPI solubility coefficients were 97 ± 3, 88 ± 7, and 92 ± 6 cm^3 (STP) cm^{-3} bar^{-1} for 6FDA-6FpDA, 6FDA-6FmDA, and 6FDA-DAM, respectively. Compared to the corresponding values obtained using the Lorentz−Berthelot combination rules (Tables 1−3) these are between 20% and 25% lower, which is significant but still somewhat higher than the experimental values.

A further question in the case of the three-site model of carbon dioxide is the value chosen for the partial charge on the carbon atom, which by electroneutrality sets the value for the oxygens, $q_O = -q_C/2$. This value is optimized to best represent the properties of pure carbon dioxide.[108] It is not obvious, however, whether the same value should be used in the case of infinite dilution where the CO_2 molecule is only surrounded by the polymer. Although it might be feasible to perform *ab initio* calculations to estimate the influence of the local environment on the charge distribution, an idea of the

Table 4. Influence of the Partial Charge Distribution in the Three-Site Model of Carbon Dioxide on the Solubility Coefficient[a]

charge scaling factor/%	q_C/e	q_O/e	TPI solubility/cm^3 (STP) cm^{-3} bar^{-1}
100	0.58880	−0.29440	122
90	0.52992	−0.26496	102
80	0.47104	−0.23552	89
70	0.41216	−0.20608	79
0	0	0	55

[a] The results of EVMS TPI calculations on just one pure relaxed system of 6FDA-6FpDA at 308 K are shown.

dependence of the solubility on this parameter can be obtained by simply scaling down the partial charges on the CO_2 molecule used as the test particle in the TPI calculations on the pure polymers. The results of some tests on just one system of a relaxed 6FDA-6FpDA system at 308 K are shown in Table 4. Scaling down the charges naturally reduces the interactions with the polymer atoms and leads to lower solubilities. However, even if the partial charges are set to zero, the solubility is still overestimated. Considering that experimental measurements of the quadrupole moment of CO_2 in the gas phase lead to even higher estimates of the partial charge on the oxygen atoms of $-0.32e$,[127] it seems unlikely that this can be the prime cause.

When compared to simulated values, there are also many factors affecting experimental data. In the literature, it is largely accepted that the solubility of gas molecules in polymer membranes is governed by the hole-filling mechanism at low gas pressures.[41,42,128] The amount of fractional free volume (FFV) available for gas sorption is the principal factor determining the solubility at low pressures.[41,42] In molecular models, we can be certain that the FFV is completely available for CO_2 sorption. In experiments, however, it is possible that residual solvent molecules, or other contaminants, are present inside the membrane, and these ultimately reduce the amount of CO_2 sorption.[129−131] Other experimental factors such as the preparation method, the solvent used to cast polymer membranes, and thermal treatments also have an impact on FFV and hence on solubility.[43,44,84] Another key issue is the physical aging of polymers, which generally leads to densification as the nonequilibrium free volume is gradually reduced.[132] Experimentally, the consequences of this have been measured in terms of the drop in solubility of CO_2 in aged samples of, for example, 6FDA-durene polyimide[133] and polycarbonate[134] and correlated to the reduction of the Langmuir component of the solubility. In these cases, changes in solubility are at least of the order of 10% over aging periods ranging from hundreds of hours to hundreds of days. It is not easy, however, to determine from these results the effects physical aging has on going from the MD simulation time scale of a few nanoseconds to a real experimental time scale of a few hours or days. Attempts to address this issue have been made using molecular simulations by generating polymer models at different densities corresponding to the known age-dependent experimental densities.[135] However, the correspondence between generating samples at different densities and then simulating them under constant volume conditions in order to maintain the initial density, i.e., at different pressures, and true physical aging, i.e., samples held at constant pressure for long periods and likely to undergo structural changes, is not at all obvious. Such studies are more equivalent to studying the pressure dependence of solubility on freshly generated samples. In this work, one sample of 6FDA-6FpDA was subjected to a cycle of annealing (heating to 508 K and cooling back to 308 K) under NPT conditions. This led to a decrease

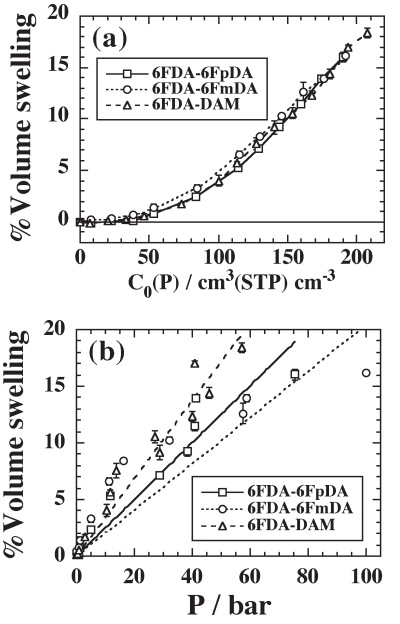

Figure 6. Average volume swelling induced at 308 K in the models of 6FDA-6FpDA, 6FDA-6FmDA, and 6FDA-DAM by sorption of CO_2 plotted as a function of (a) the (pressure-dependent) nominal concentration of CO_2 and (b) the pressure. The lines in (b) are linear least-squares fits to the form of eq 15. For clarity, the error bars on the pressure have been omitted from (b).

of ∼13% in the solubility. Although this could indicate that aging can be addressed at least in some respect with MD simulations, this would require a more thorough investigation which is beyond the scope of this article. Until this problem is tackled in a more satisfactory way, it will remain difficult to quantify the effect aging from the nanosecond to experimental time scales has on solubility of gases in amorphous polymers. In this respect physical aging remains a factor that could well explain, at least in part, the discrepancies in the limiting low concentration solubilities.

4.2. Volume Swelling. Penetrant-induced volume dilation is known to occur in the case of carbon dioxide sorption in glassy polymers.[136] Dilation experiments are often performed using a different apparatus than the sorption experiments so measuring volume changes with respect to gas concentration is inevitably subject to some added uncertainty.[38,88,137] However, Wang et al.[138−140] have made concurrent measurements of sorption, dilation, and diffusion of CO_2 in polysulfone and poly(benzyl methacrylate), and Hölck et al. have performed a concurrent sorption and dilation measurement of CO_2 in 6FDA-DAM at 308 K at a pressure of 10 bar.[79]

In simulations carried out in periodic boundary conditions the dilation can be measured as a function of mass uptake directly. The volume swelling induced by CO_2 is directly measured from the differences in volumes of the polymer matrices containing different concentrations of CO_2 with respect to the pure polyimide matrices.

$$\%\ \text{volume swelling} = \frac{V(P) - V_0}{V_0} \times 100 = \frac{\Delta V(P)}{V_0} \times 100 \qquad (13)$$

Figure 6a shows the relative volume swelling during loading of the different systems as a function of the nominal concentration of CO_2.

In general, the swelling behavior as a function of the gas concentration in these model polyimides is one in which the initial gas uptake causes little volume expansion. Thereafter, there is a gradual transition to an almost linear increase in volume at higher concentrations. The slight differences between the model polymers in the volume swelling vs concentration curves can be attributed to the differences in their FFV.[73,128] The denser packing and lower FFV (0.167)[73] of the 6FDA-6FmDA polyimide leads to a slightly higher volume dilation in the low and intermediate CO_2 concentration range. With a higher FFV (0.176)[73] 6FDA-6FpDA dilates less than the 6FDA-6FmDA isomer in the same concentration range. In 6FDA-DAM the packing is disrupted by the methyl substituents in the diamine part that give rise to the highest FFV (0.178)[73] of the three, but this is only marginally higher than that of 6FDA-6FpDA and does not lead to significant differences in volume swelling. At the higher concentrations the volume swelling behavior seems to converge. The limiting slopes at high concentration can be related to the partial molar volume of CO_2

$$\frac{\partial V(n)}{\partial n} = \frac{\partial\left(\frac{\Delta V}{V_0}\right)}{\partial C}\frac{RT^{STP}}{P^{STP}} \tag{14}$$

and within errors these are all about 30 ± 2 cm^3 mol^{-1} in the three polyimides. This value is somewhat lower than the average partial molar volume of CO_2 in a number of organic solvents of 46 cm^3 mol^{-1}.[141] However, it is very similar to the range of values (27−31 cm^3 mol^{-1}) reported for 6FDA-DAM-based cross-linked copolymers[45] and compares well also to the values found at short times for the dilation of polysulfone and poly(ether sulfone).[137]

To our knowledge the only published experimental data concerning the CO_2-induced volume dilation of any of the three particular polyimides studied here is the one concurrent sorption and dilation measurement made on 6FDA-DAM by Hölck et al. at a pressure of 10 bar and at a temperature of 308 K.[79] Their result of 6.13% volume dilation compares to our value of ∼4% at a pressure of ∼10 bar. However, if the comparison is made at the same nominal concentration of CO_2 instead (∼80 cm^3 (STP) cm^{-3}), then our result is somewhat lower at ∼2%. The greater amount of swelling seen in experiment is consistent with other findings. Wessling et al. have carried out separate dilation and sorption experiments on related 6FDA-based polyimides.[88] They find that dilation starts at very low nominal concentrations, ∼10 cm^3 (STP) cm^{-3}, based on an extrapolation to zero dilation of the data given in Figure 5c of ref 88. It reaches values of ∼3% at a nominal concentration of ∼50 cm^3 (STP) cm^{-3} compared to about 80−90 cm^3 (STP) cm^{-3} in the model systems (Figure 6a). It is not possible to say whether the fact that the sorption and dilation experiments were done separately, with a different pressure loading protocol, influenced the results. Concurrent measurements of sorption and dilation of CO_2 by polysulfone and poly(benzyl methacrylate) also indicate that, on the experimental time scale, dilation occurs immediately.[138−140] There are fundamental differences, however, between the experiments and the simulations in the way the loading is performed. In the experiments the CO_2 enters the membrane from the exterior and has to diffuse through the macroscopic sample, whereas in the simulations the CO_2 is inserted directly at the most favorable sites. Once inserted though, the CO_2 molecules are free to, and do, diffuse, thus diminishing the importance of where they are initially inserted. Another factor that cannot be discounted is the different time scales involved. These are inevitably short in simulations with respect to experiments for which it is known that penetrant-induced volume relaxation can be extremely slow.[88,137]

It has previously been argued that if the Langmuir sorption term in the DMS model corresponds to a true hole-filling process, then its effect on the volume dilation of the polymer should be negligible.[141] Volume dilation can then be attributed just to the number of moles of gas truly "dissolved" in the polymer matrix; from eq 12 this is simply proportional to $k_D P$. Assuming that the partial molar volume of CO_2, V_{CO_2}, is independent of pressure, this gives the following prediction for the volume dilation[141]

$$\frac{\Delta V}{V_0} = \frac{k_D P}{RT^{STP}/P^{STP}} V_{CO_2} = \frac{k_D P}{22414\ \text{cm}^3} V_{CO_2} \tag{15}$$

Equation 15 has been found to predict reasonably well the CO_2-induced volume dilation of polycarbonate using a value of V_{CO_2} = 46 cm^3 mol^{-1}.[141] For this reason the data for volume swelling has also been plotted as a function of the pressure in Figure 6b. The data for 6FDA-6FpDA and 6FDA-DAM show some scatter about the best fit lines to the form of eq 15, but it is clear that 6FDA-6FmDA shows a systematic deviation. Despite this the resulting linear least-squares best fit values for V_{CO_2} were 47 ± 9, 65 ± 13, and 38 ± 4 cm^3 mol^{-1} for 6FDA-6FpDA, 6FDA-6FmDA, and 6FDA-DAM, respectively. These do not compare particularly well to the common value of 30 ± 2 cm^3 mol^{-1} determined directly from the volume swelling vs nominal concentration curve. In addition, nonlinear behavior of the volume swelling with CO_2 vapor pressure has been found in 6FDA-DAM-based cross-linked copolymers,[45] 6FDA-based polyimides,[88] and polysulfone and poly(ether sulfone).[137] Such nonlinear behavior has led to the development of more elaborate models to describe swelling based on a continuous distribution of hole sizes.[142,143]

From Figure 6a it is clear that the effective volume dilation starts above a nominal concentration of ∼50 cm^3 (STP) cm^{-3} for all three polyimides under study. Experimentally, the plasticization pressure of glassy polymers is defined as the point where the permeability passes through a minimum, thus the point at which the increasing diffusivity compensates for the decreasing solubility of the penetrant. Bos et al.[38] studied 11 different glassy polymers and reported that all the polymers are plasticized at about the same critical (nominal) concentration of 36 ± 7 cm^3 (STP) cm^{-3}. However, from the actual experimental CO_2 permeability and mass uptake curves reported by Coleman et al.,[41] a higher critical concentration of 57 cm^3 (STP) cm^{-3} was estimated for both 6FDA-6FpDA and 6FDA-6FmDA. In the case of 6FDA-DAM, from similar curves reported by Wind et al.,[144] a critical concentration of ∼77 cm^3 (STP) cm^{-3} was calculated. This apparent correlation between the start of effective volume dilation in the models and the experimentally determined critical concentrations for plasticization may well be just a coincidence. Although we might expect some correlation between the solubility and volume swelling, it is less evident that there would be a correlation with plasticization.

4.3. Void Space. The void space analysis of the polyimides as a function of CO_2 concentration was carried out using a simple geometric technique, and the probe accessible volume (PAV) was calculated. This method is similar to various other phantom sphere approaches commonly found in atomistic simulations, and the details of this specific method can be found elsewhere.[105] In brief, the PAV was obtained from repeated random insertions of a virtual probe of radius of 1.8 Å into the MD simulation boxes having different loadings

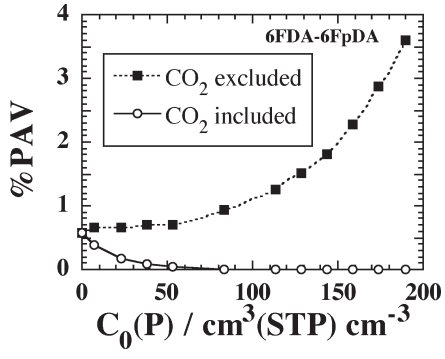

Figure 7. Probe accessible volume (PAV) expressed as a percentage of the pure polymer volume for one system of 6FDA-6FpDA at 308 K. The PAV has been obtained by both including and excluding the CO_2 molecules present in the system.

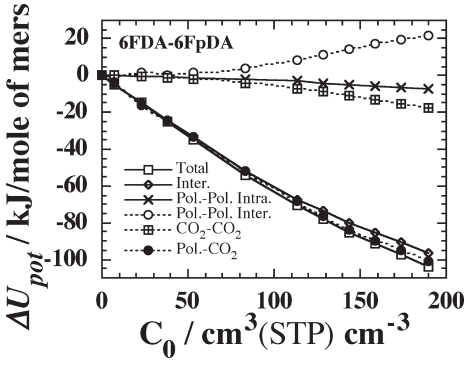

Figure 8. Changes in the total potential energy, and its resolution into the different contributions, with respect to the pure polymer as a function of the nominal concentration of CO_2 at 308 K for 6FDA-6FpDA. Energy changes are quoted in kJ/mol of mers.

of CO_2. The PAV was calculated in two ways by taking into account or not the actual CO_2 molecules present in the system. In the case where CO_2 molecules were excluded, all polymer atoms in the simulation boxes were treated as hard spheres with standard van der Waals radii (1.20 Å for H, 1.35 Å for F, 1.50 Å for O, 1.55 for N, and 1.70 Å for C), whereas the carbon dioxide molecules present were ignored. A random trial insertion was then "accepted" if the probe sphere did not overlap with any of the polymer atoms in the simulation box. The PAV is then calculated simply as the fraction of "accepted" insertions with respect to the total number of trials multiplied by the volume of the box. It is important to point out that, as such, the PAV is just the volume accessible to the *centers* of the virtual probes. This method does not make any attempt to calculate the total volume accessible to the virtual probe and is just intended to give relative comparisons between similar systems. In the case where the CO_2 molecules actually present in the system were considered the C and O atoms were given the same standard hard-sphere radii as given above. These two calculations of the PAV give different information about the space available.

An illustration of the typical results obtained is shown in Figure 7 where the PAV is shown as a function of the nominal CO_2 concentration for just one system of the 6FDA-6FpDA polyimide; all systems were qualitatively similar in their behavior. At nominal concentrations of CO_2 less than ~50 cm^3 (STP) cm^{-3} the CO_2-excluded PAV hardly changes whereas the CO_2-included PAV gradually diminishes as holes are filled up. Above this critical concentration the CO_2-included PAV remains very small, whereas the CO_2-excluded PAV reflects the same behavior as the volume swelling curve (Figure 6a).

The distributions of PAV hole sizes were also analyzed by using a cutoff distance of 0.5 Å to identify all accepted probe centers falling into the same hole. Although not shown here, the CO_2-excluded PAV hole size distributions remain similar below the critical concentration of CO_2. This also clearly indicates the domination of hole-filling sorption at low concentrations, there being no new holes formed in this regime. Above the critical concentration of CO_2, the percentage of smaller holes is diminished and the percentage of larger holes is increased.

4.4. Energy and Entropy. The changes in the average total potential energy, ΔU_{pot}, of the different CO_2-containing systems, relative to the pure polymers, have been calculated and resolved into their component parts. Figure 8 shows these various contributions to the ΔU_{pot} as a function of the nominal CO_2 concentration in the case of 6FDA-6FpDA. The results for 6FDA-6FmDA are quantitatively very similar to 6FDA-6FpDA, and although 6FDA-DAM shows slight differences qualitatively, the trends are the same. The change in total potential energy is negative, i.e., exothermic, as reported in the literature.[85] At low concentrations ΔU_{pot} decreases almost linearly with the major contribution being the polymer−CO_2 interactions. The onset of volume swelling, above $C_0 \sim 50$ cm^3 (STP) cm^{-3}, coincides with a less steep decrease in the polymer−CO_2 contribution and changes in the polymer−polymer interactions. The intermolecular polymer−polymer contribution becomes less cohesive, as chains become further apart, while a slight decrease in the polymer−polymer intramolecular contribution counterbalances this. The gradual change in the CO_2−CO_2 contribution also nullifies the loss in the polymer−polymer cohesive energy.

The two contributions to the excess chemical potential, i.e., the excess molar enthalpy (h_{ex}) and the excess molar entropy (s_{ex}), were also estimated. To obtain estimates of h_{ex} the average values of $U_{pot} + PV$, i.e., total enthalpy minus the kinetic energy contribution, from the simulations carried out at 1 bar were plotted as a function of the number (n) of added CO_2 molecules. The resulting curves were then fitted to a combination of two linear functions

$$H(n) = (a + bn)(1 - S(n)) + (C + dn)S(n) \qquad (16)$$

where a, b, c, and d are constants and $S(n)$ is a switching function which goes from 1 to 0 in a controllable interval either side of a critical number of added CO_2 molecules, n_c. In this work the following form for $S(n)$ has been chosen

$$S(n) = \frac{1}{2}\left(1 + \frac{n - n_c}{\omega + |n - n_c|}\right) \qquad (17)$$

where ω is a variable parameter controlling the sharpness of the switching function; $\omega = 0$ being the standard Heaviside function. It seems reasonable to assume that the initial addition of CO_2 leads to a linear change in the enthalpy, the volume swelling being small initially this is effectively confirmed by Figure 8, and at high CO_2 concentration it should become linear again too as it tends toward a pure CO_2 system. The resulting smooth curves (not shown) gave excellent fits to the data, and the excess molar enthalpies were then obtained from the analytical derivation of eq 16 and the best fit coefficients. The estimation of the derivatives in this way was consistent with numerical estimates using simple difference equations but were much smoother. Once

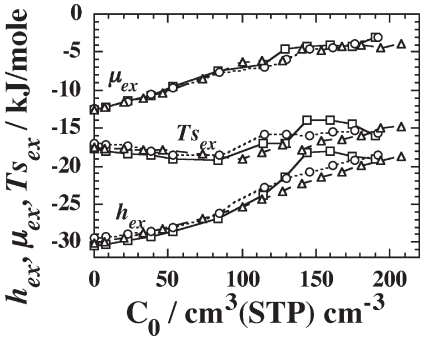

Figure 9. Excess molar enthalpy (h_{ex}), excess molar entropy (s_{ex}), and the excess chemical potential (μ_{ex}) plotted as a function of the nominal CO_2 concentration in the respective polymer matrices. Squares represent 6FDA-6FpDA, circles 6FDA-6FmDA, and triangles 6FDA-DAM.

the h_{ex} have been obtained, the excess molar entropies can be estimated indirectly using the following equation

$$Ts_{ex} = h_{ex} - \mu_{ex} \tag{18}$$

All three excess molar properties are plotted for all three systems in Figure 9 as a function of the nominal CO_2 concentration.

The excess molar enthalpies gradually decrease from an initial value of about −30 kJ/mol to a value of about −20 kJ/mol as CO_2 concentration increases. This latter value is more negative compared to those typical of pure liquid CO_2, e.g., about −17 kJ/mol at 290 K as seen in section 2.7, confirming the predominance of polymer−CO_2 interactions (see Figure 8) in the regime of concentrations studied. The behavior of the excess molar chemical potential seems to mirror that of h_{ex} initially, but at higher concentrations there are signs of a plateau at $\mu_{ex} \approx -4$ kJ/mol. This value is already slightly above that for dense pure liquid CO_2 of −6 kJ/mol, albeit at a lower temperature of 290 K, or the supercritical (dense) fluid value of about −5 kJ/mol of CO_2 in the 100−200 bar range of pressure at 308 K. This can be explained by the behavior of the Ts_{ex} term which we interpret as being consistent with the behavior of the partial molar volume of added CO_2. Initial hole filling leads first to a slight descent to more negative values in the entropic contribution, but once the volume swelling starts to accelerate, this trend is reversed and Ts_{ex} begins to rise as each CO_2 has to create its own space in the system. The values of Ts_{ex} are still some way off that of about −11 kJ/mol typical of pure liquid CO_2 at 290 K, but this is consistent with the partial molar volume still being less than that in pure CO_2, too.

According to the site-distribution model of Kirchheim,[142,143,145−147] the sorbed gas molecules fill the low-energy microvoids initially, and then the polymer has to adjust itself to adopt more gas molecules. Gas insertion energies thus increase with the increasing concentration of gas molecules. This hypothesis can be tested to a certain extent by analyzing the distribution of CO_2 insertion energies obtained from the TPI calculations carried out at different concentrations of CO_2 in the polymer matrices. The normalized probability density distribution of insertion energies that results from TPI, $\rho(\Delta\Phi)$, necessarily contains information concerning those trial insertions which are of high energy, thus of low probability. To obtain a distribution more representative of the energy of likely sites of adsorption, this distribution is weighted by the associated Boltzmann factor, i.e., $\rho_\omega(\Delta\Phi) = \rho(\Delta\Phi)\exp(-\Delta\Phi/kT)$. Examples of these weighted probability density functions are shown in Figure 10 in the case of 6FDA-6FpDA at a range of CO_2 concentrations.

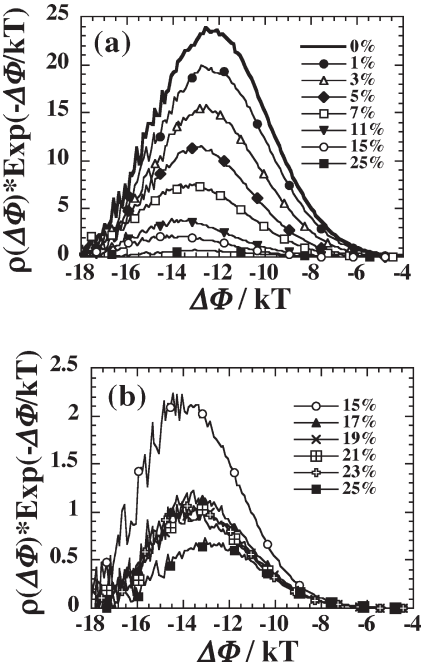

Figure 10. Boltzmann-factor-weighted probability density distributions for the insertion energy of a virtual probe CO_2 molecule in the three 6FDA-6FpDA systems containing different concentrations of CO_2. The lower figure shows the concentrations in the range from 15 to 25% on an enlarged scale.

The resulting weighted insertion energy distributions are smooth and single-Gaussian-like with no signs of a bimodal distribution, as was recently shown by a molecular study of oxygen sorption in polyimides.[101] They thus support the site-distribution model rather than the dual-sorption model. However, the weighted distributions also show a fairly homogeneous and progressive reduction in the number of sites available for adsorption. There is no obvious indication that the lower energy sites are being filled in preference. Indeed, the peak in the distributions moves, if anything, toward lower energies in the range from 0 to 15%. We attribute this to the increasing quantity of CO_2 in the system in the phase before volume swelling becomes important. If the rubbery state had been attained, where Henry's law is obeyed, no further shift in $\rho_\omega(\Delta\Phi)$ would be expected at the higher loadings. The results shown for the higher concentrations in Figure 10b seem to indicate that above 15% there is a tendency for the distributions to differ less with a gradual shift of the maximum to lower energies. A closer inspection of the data for the individual samples (not shown) reveals that the apparent break between 23 and 25% in 6FDA-6FpDA is not due to anything peculiar with the 25% systems but is due to one sample having higher values for the 21 and 23% systems than the other two samples. The underlying trend, at least in the range of concentrations simulated, is thus always toward a gradual decrease in these distributions with an ever decreasing gap. This is in agreement with the behavior of the solubility with increased concentration, with which there is a clear connection since $\left\langle \exp\left(-\frac{\Delta\phi}{kT}\right)\right\rangle = \int_{-\infty}^{+\infty} \rho(\Delta\phi)\exp\left(-\frac{\Delta\phi}{kT}\right) d\Delta\phi$. The distributions for the other two polyimides (not shown) confirm this trend.

4.5. Cluster Analysis. The possibility of formation of CO_2 clusters was analyzed. Two molecules were deemed to be in the same cluster if the distance between the carbon atom of one molecule was within a distance of 3 Å of an oxygen atom of the other molecule. This distance was obtained by trial and

error but roughly corresponds to the first peak in the radial distribution function. The average results obtained for the distribution of cluster sizes from the MD simulations of 25% CO_2 in 6FDA-6FpDA system are displayed in Figure 11.

For comparison, the distribution obtained in the pure gas phase at same density of CO_2 (322.33 kg m^{-3}), i.e., from simulations using the same size of MD box as the 25% CO_2 in 6FDA-6FpDA system having first removed the polymer. As might be expected from the restricted space available to the CO_2 molecules in the polymer plus CO_2 system, the percentage of single CO_2 molecules in the polymer phase is less than that in the gas phase. However, there is no obvious formation of large clusters which suggests that the CO_2 molecules tend to rest apart even in the polymer phase. Similar cluster distributions were found in the other two polyimides under study. This is also supported by the results for the potential energy (Figure 8) which show a fairly feeble contribution of $CO_2 \cdots CO_2$ interactions to the total potential energy.

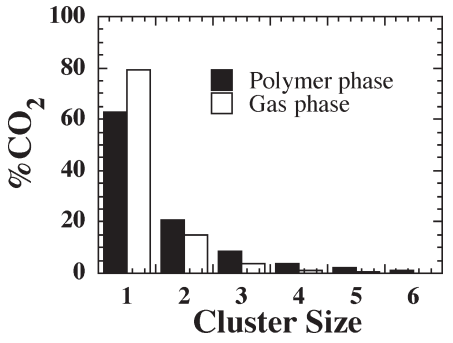

Figure 11. Percentage of CO_2 molecules in clusters of a given size in the 6FDA-6FpDA system containing ~25% of CO_2 compared to the distribution obtained from simulation of a pure gas phase CO_2 system at the same CO_2 density (see text for details).

5. Carbon Dioxide Unloading from Polyimides

The effect of penetrant-induced hysteresis (conditioning) under various CO_2 feed pressures has been reported in the literature for the 6FDA-6FpDA and 6FDA-6FmDA polyimides.[41,42] In these real experiments the conditioning was carried out at different gas pressures, up to ~60 bar, and for times of 2−3 weeks; such long times are necessary to attain "steady state" where permeabilities changed less than 0.5% per day. The experiments reveal that the significant increases in permeability after conditioning are due to increases in solubility and diffusivity, with the latter being the major cause due to enhancements caused by the volume relaxations and polymer chain mobilities.[41,42] Even though it is impossible to study the effects of such a long-term conditioning, given current limitations of MD simulations, it is still nevertheless interesting to check the immediate effect of exposure to high concentrations of CO_2 in polymers. As explained in section 2.6, unloading curves were produced in a similar manner to the loading curves this time by stepwise removal of the CO_2 molecules from systems exposed to a pressure of ~60 bar. Just one system for each type of polyimide was studied in this way.

Tables 5−7 show the nominal and true solubility of CO_2 calculated from the iterative and TPI procedures. The comparable values obtained between iterative and TPI solubilities once again confirms the reliability of the former procedure. Figure 12 shows a comparison of the nominal solubility vs pressure curves for the sorption and desorption isotherms in the case of 6FDA-DAM. On the log−log scale of Figure 12 only a slight tendency for an increase in solubility is observed during desorption. The trend is the same in the other two polyimides (plots not shown), but differences are even less. This is not to say that there are no

Table 5. Desorption Isotherm MD Simulations at 308 K on 6FDA-6FpDA[a]

~% CO_2	no. of CO_2	true concn $V_g^{STP}(P)/V(P)$	nominal concn $V_g^{STP}(P)/V_0$	P/bar	true solubility $C(P)/P$	nominal solubility $C_0(P)/P$	TPI solubility
24.33	616	184.23	163.22	45.70	3.57	4.03	3.36
23	582	174.07	153.12	37.20	4.12	4.68	3.99
21	531	158.81	142.41	23.75	6.00	6.69	5.85
19	481	143.86	131.64	17.20	7.65	8.36	7.68
17	430	128.60	119.91	11.40	10.52	11.28	10.62
15	380	113.65	107.41	6.15	17.46	18.48	17.01
11	278	83.14	80.88	2.75	29.41	30.23	27.95
7	177	52.94	52.34	1.20	43.61	44.11	46.17
5	127	37.98	37.86	0.60	63.11	63.31	64.31
3	76	22.73	22.68	0.23	98.63	98.83	95.69
1	25	7.48	7.48	0.07	115.04	115.03	117.32
0	0	0.00	0.00				137.63

[a] The approximate mass percentages of CO_2 are given as obtained from the actual number of molecules inserted into the polymers. The corresponding true and nominal concentrations of gas in the polymer are shown in units of cm^3 (STP) cm^{-3} of polymer (true or pure polymer volume). The pressure given is that estimated to be the equilibrium external vapour pressure of CO_2 which would have to be applied to give the imposed concentrations of CO_2 in the polymer. The true and nominal solubility coefficients are given as well as the solubility coefficient estimated from the EVMS test particle insertion analysis (eq 10 or 11) in units of cm^3 (STP) cm^{-3} bar^{-1}.

Table 6. As Table 5 for 6FDA-6FmDA

~% CO_2	no. of CO_2	true concn $V_g^{STP}(P)/V(P)$	nominal concn $V_g^{STP}(P)/V_0$	P/bar	true solubility $C(P)/P$	nominal solubility $C_0(P)/P$	TPI solubility
23	582	176.00	153.63	42.00	3.66	4.19	4.33
21	531	160.58	140.31	38.90	3.61	4.13	4.79
19	481	145.46	131.65	25.80	5.10	5.64	5.61
17	430	130.03	119.52	16.10	7.42	8.08	8.08
15	380	114.91	107.30	10.25	10.47	11.21	10.81
11	278	84.07	81.06	3.30	24.56	25.48	24.51
7	177	53.53	52.74	1.15	45.86	46.54	44.56
5	127	38.41	38.05	0.55	69.18	69.83	70.02
3	76	22.98	22.92	0.26	88.17	88.39	84.53
1	25	7.56	7.53	0.07	109.19	109.57	109.93
0	0	0.00	0.00				127.68

Table 7. As Table 5 for 6FDA-DAM

~% CO_2	no. of CO_2	true concn $V_g^{STP}(P)/V(P)$	nominal concn $V_g^{STP}(P)/V_0$	P/bar	true solubility $C(P)/P$	nominal solubility $C_0(P)/P$	TPI solubility
31	589	209.27	176.15	74.15	2.38	2.82	1.36
29	551	195.77	165.99	43.80	3.79	4.47	2.85
27	513	182.27	155.57	31.00	5.02	5.88	5.72
25	475	168.76	145.82	21.95	6.64	7.69	5.84
23	437	155.26	135.73	12.28	11.05	12.64	10.52
21	399	141.76	124.90	9.95	12.55	14.25	11.63
19	361	128.26	113.36	5.39	21.03	23.80	19.58
17	323	114.76	102.81	5.01	20.52	22.91	19.10
15	285	101.26	92.56	4.20	22.06	24.14	20.69
11	209	74.26	68.48	1.93	35.48	38.47	33.20
7	133	46.90	44.25	0.74	60.21	63.81	51.22
5	95	33.75	31.62	0.43	73.54	78.49	69.01
3	57	19.90	18.97	0.20	96.81	101.51	90.52
1	19	6.75	6.33	0.05	126.55	135.01	123.26
0	0	0.00	0.00				147.59

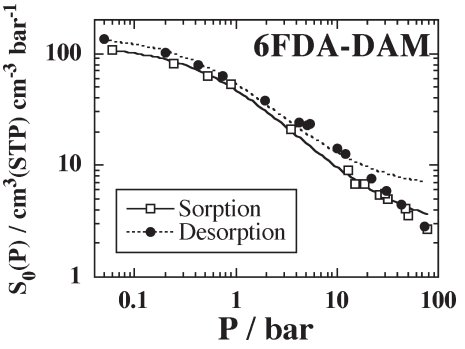

Figure 12. Comparison of CO_2 sorption and desorption isotherms obtained from just one sample of 6FDA-DAM at 308 K. The solubility coefficients are plotted as a function of nominal concentrations of carbon dioxide (eq 9) on a log−log scale. Lines are nonlinear least-squares regression fits to the solubility form of the dual mode sorption model (eq 12).

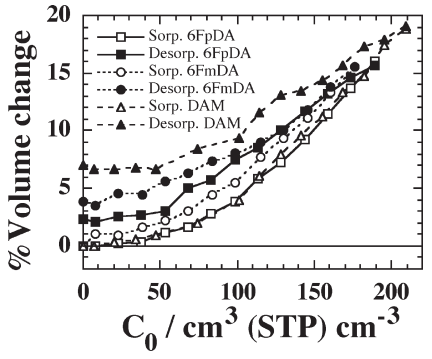

Figure 13. A comparison of volume swelling during sorption (open symbols) and volume contraction during desorption (filled symbols) for all three polyimides at 308 K as obtained from the simulations reported here. The percentage volume change relative to the original pure polyimide systems prior to the sorption of CO_2 are plotted as a function of nominal concentrations of carbon dioxide (eq 9).

immediate conditioning effects when the polymer membrane is exposed to high pressure of CO_2. There are compensating changes taking place which mean that the nominal solubility vs pressure curves are not the best way to reveal them. To demonstrate this, the volume contractions during desorption were also calculated directly from the volume of the MD simulation boxes. Figure 13 shows the volume dilations and contractions relative to the original pure polyimide systems, i.e., prior to any sorption of CO_2, as a function of nominal concentration of CO_2. The differences between dilation and contraction curves can be explained by the volume relaxations induced by the higher concentrations of CO_2.[79,143] From Figure 13 it is clear that the 6FDA-DAM has the least amount of volume contraction as it shows almost 7% volume change at the end of complete desorption of CO_2, whereas the 6FDA-6FpDA and 6FDA-6FmDA exhibit close to 2.5 and 4% induced volume changes, respectively.

6. Conclusion

MD simulation techniques have been successfully used to obtain sorption isotherms of CO_2 in three different polyimides: 6FDA-6FpDA, 6FDA-6FmDA, and 6FDA-DAM. For the first time, a simple iterative technique to obtain the sorption isotherm[81] has been applied to realistic models of polyimides. The method is robust and converges rapidly. Both CO_2 loading and unloading curves were obtained. An excluded volume map sampling test particle insertion technique was found to be an efficient method to calculate the excess chemical potentials required for the iterative approach.

Although the solubilities in the infinite dilution limit predicted from the simulations were found to be significantly higher than those extrapolated to zero pressure from experimental data, at pressures of 10 bar the predicted solubilities are within a factor of 2 of the experimental results. The simulations also reproduce the experimental order in the solubilities of the three polyimides, but the two structural isomers, 6FDA-6FpDA and 6FDA-6FmDA, are closer in behavior than is found in reality. Explanations for the overestimation of infinite dilution solubilities in terms of the details of the potential models were sought, but none of those tested could account for the discrepancies. In particular, the considerably higher solubilities obtained using a united-atom models of CO_2 suggest that this purely spherical representation of CO_2 is poorly adapted for such studies.

All three polyimides swell significantly and homogeneously during CO_2 sorption. There is no evidence to suggest that large clusters of CO_2 form even at the highest concentrations. Initial gas uptake causes little volume expansion, i.e., consistent with a hole-filling mechanism, but thereafter there is a gradual transition to an almost linear increase in volume at higher concentrations. These results were consistent with the determinations of the probe accessible volumes. Where comparisons with swelling in experimental systems were available, significant swelling in the models started at higher concentrations and so was less consequent when compared at the same concentration of CO_2.

Analysis of the changes in the contributions to the total potential energy reveal that the interactions between the polymer and the carbon dioxide are largely responsible for the change. Other contributions exist but tend to cancel out. The excess molar enthalpies and excess molar chemical potentials show trends with increased concentration consistent with a progression from a

pure polyimide system to a pure dense CO_2 system. The associated excess molar enthalpy also shows trends consistent with an initial hole-filling behavior followed by increased volume swelling. The Boltzmann factor weighted probability density distributions for the trial insertion energies show a single Gaussian-like peak. Although this could be thought to be supportive of the site-distribution model, rather than the dual sorption model, there is no evidence to suggest that the lower energy microvoids are filled preferentially. Indeed, the weighted distributions remain Gaussian-like and diminish homogeneously with concentration.

Immediate desorption following sorption leads to relatively small increases in the solubilities compared to those obtained in the laboratory through very long conditioning protocols. However, the models do predict significant changes in volume of the pure polymers following complete outgassing of the samples.

In this work, we addressed several key issues related to the solubilities, volume changes, void space characterizations, and energetic properties in glassy polyimides as a function of CO_2 concentration. Such molecular models can also bring insight related to diffusion of the penetrant within the polymer matrices. Detailed analyses of diffusivities at different CO_2 loadings will consequently be reported in a second article.

Acknowledgment. This work was granted access to the HPC resources of CCRT/CINES/IDRIS under the allocation 2009-095053 made by GENCI (Grand Equipement National de Calcul Intensif), France. The MUST cluster at the University of Savoie (France) and the MPIP (Germany) are also acknowledged for their generous provision of computer time. S.P. is deeply grateful to the Assemblée des Pays de Savoie and to the MPIP for the award of a doctoral research grant as well as to the Région Rhône-Alpes for the award of a travel grant.

Appendix

The chemical potential at a certain higher pressure, P', can always be obtained by integration along an isotherm[102]

$$\mu(P',T)=\mu(P_{\text{low}},T)+\int_{P_{\text{low}}}^{P'}\left(\frac{\partial\mu}{\partial P}\right)_T \mathrm{d}P \tag{A1}$$

where P_{low} is some reference "low" pressure and $\mu(P_{\text{low}},T)$ the corresponding chemical potential. The partial derivative of the chemical potential with respect to pressure at constant temperature is just $1/\rho = V/N$.[102] So we can write

$$\mu(P',T)=\mu(P_{\text{low}},T)+\int_{P_{\text{low}}}^{P'}\frac{V(P,T)}{N}\mathrm{d}P \tag{A2}$$

Adding and subtracting a term kT/P, corresponding to the volume of the ideal gas divided by N, to the integral gives

$$\begin{aligned}\mu(P',T) &= \mu(P_{\text{low}},T)+\int_{P_{\text{low}}}^{P'}\frac{V(P,T)}{N}-\frac{kT}{P}+\frac{kT}{P}\mathrm{d}P\\ &= \mu(P_{\text{low}},T)+\int_{P_{\text{low}}}^{P'}\frac{V(P,T)}{N}-\frac{V^{\text{ig}}(P,T)}{N}\mathrm{d}P+\int_{P_{\text{low}}}^{P'}\frac{kT}{P}\mathrm{d}P\\ &= \mu(P_{\text{low}},T)+\int_{P_{\text{low}}}^{P'}\frac{V(P,T)}{N}-\frac{V^{\text{ig}}(P,T)}{N}\mathrm{d}P+kT[\ln P]_{P_{\text{low}}}^{P'}\\ &= \mu(P_{\text{low}},T)+kT\ln\frac{P'}{P_{\text{low}}}+\frac{1}{N}\int_{P_{\text{low}}}^{P'}V(P,T)-V^{\text{ig}}(P,T)\,\mathrm{d}P\end{aligned} \tag{A3}$$

To obtain the chemical potential at the low pressure, we use the standard statistical mechanics expression for the chemical potential in the NPT ensemble[102,104]

$$\mu=kT\ln\frac{\rho\Lambda^3}{q}-kT\ln\frac{\left\langle V\exp\left(\frac{-\Delta U}{kT}\right)\right\rangle}{\langle V\rangle}=\mu_{\text{id}}+\mu_{\text{ex}} \tag{A4}$$

where q is the partition function for internal degrees of freedom and Λ is the de Broglie wavelength defined as

$$\Lambda=\left(\frac{h^2}{2\pi mk_{\text{B}}T}\right)^{1/2} \tag{A5}$$

with h being Planck's constant and where it is understood that the number density $\rho = N/\langle V\rangle \approx (N+1)/\langle V\rangle$ is that corresponding to the applied conditions of P and T, i.e., $\rho = \rho(P,T)$. Now for the reference state we choose a pressure *sufficiently low* that the ideal gas law holds then the chemical potential is well approximated by the first term in eq A4 and thus

$$\mu(P_{\text{low}},T)\approx kT\ln\left[\frac{\rho(P_{\text{low}},T)\Lambda^3}{q}\right]\approx kT\ln\left[\frac{P_{\text{low}}\Lambda^3}{qkT}\right] \tag{A6}$$

Equation A3 can then be written as

$$\begin{aligned}\mu(P',T) &= kT\ln\left[\frac{P_{\text{low}}\Lambda^3}{qkT}\right]+kT\ln\frac{P'}{P_{\text{low}}}+\frac{1}{N}\int_{P_{\text{low}}}^{P'}V(P,T)-V^{\text{ig}}(P,T)\,\mathrm{d}P\\ &= kT\ln\left[\frac{P_{\text{low}}\Lambda^3}{qkT}\right]+kT\ln\frac{P'}{P_{\text{low}}}+\frac{1}{N}\int_{P_{\text{low}}}^{P'}V(P,T)-V^{\text{ig}}(P,T)\,\mathrm{d}P\\ &= kT\ln\left[\frac{P'\Lambda^3}{qkT}\right]+\frac{1}{N}\int_{P_{\text{low}}}^{P'}V(P,T)-V^{\text{ig}}(P,T)\,\mathrm{d}P\\ &= kT\ln\left[\frac{\rho^{ig}(P',T)\Lambda^3}{q}\right]+\frac{1}{N}\int_{P_{\text{low}}}^{P'}V(P,T)-V^{\text{ig}}(P,T)\,\mathrm{d}P\end{aligned} \tag{A7}$$

where we recognize that the term P'/kT is just the number density of the ideal gas, $\rho^{\text{ig}}(P',T)$. Now adding and subtracting a term of $kT\ln\rho(P',T)$gives

$$\begin{aligned}\mu(P',T) &= kT\ln\left[\frac{\rho^{\text{ig}}(P',T)\Lambda^3}{q}\right]-kT\ln\rho(P',T)\\ &+kT\ln\rho(P',T)+\frac{1}{N}\int_{P_{\text{low}}}^{P'}V(P,T)-V^{\text{ig}}(P,T)\,\mathrm{d}P\\ &= kT\ln\left[\frac{\rho(P',T)\Lambda^3}{q}\right]-kT\ln\left[\frac{\rho(P',T)}{\rho^{\text{ig}}(P',T)}\right]\\ &+\frac{1}{N}\int_{P_{\text{low}}}^{P'}V(P,T)-V^{\text{ig}}(P,T)\,\mathrm{d}P\end{aligned} \tag{A8}$$

It follows then that the excess chemical potential, *as defined by eq* A4, is given by

$$\mu_{\text{ex}}=-kT\ln\left[\frac{\rho(P',T)}{\rho^{\text{ig}}(P',T)}\right]+\frac{1}{N}\int_{P_{\text{low}}}^{P'}V(P,T)-V^{\text{ig}}(P,T)\,\mathrm{d}P \tag{A9}$$

References and Notes

(1) Forster, P.; Ramaswamy, V.; Artaxo, P.; Berntsen, T.; Betts, R.; Fahey, D. W.; Haywood, J.; Lean, J.; Lowe, D. C.; Myhre, G.; Nganga, J.; Prinn, R.; Raga, G.; Schulz, M.; Van Dorland, R. Changes in Atmospheric Constituents and in Radiative Forcing. In *Climate Change 2007: The Physical Science Basis. Contribution of Working Group I to the Fourth Assessment Report of the Intergovernmental Panel on Climate Change*; Cambridge University Press: Cambridge, UK, 2007.

(2) Sarkar, S. C.; Bose, A. *Energy Convers. Manage.* **1997**, *38* (Suppl. 1), S105–S110.

(3) Ishibashi, M.; Ota, H.; Akutsu, N.; Umeda, S.; Tajika, M.; Izumi, J.; Yasutake, A.; Kabata, T.; Kageyama, Y. *Energy Convers. Manage.* **1996**, *37* (6−8), 929–933.

(4) Kikkinides, E. S.; Yang, R. T.; Cho, S. H. *Ind. Eng. Chem. Res.* **1993**, *32* (11), 2714–2720.

(5) Cavenati, S.; Grande, C. A.; Rodrigues, A. E. *Energy Fuels* **2006**, *20* (6), 2648–2659.

(6) Ohta, H.; Umeda, S.; Tajika, M.; Nishimura, M.; Yamada, M.; Yasutake, A.; Izumi, J. *Int. J. Global Energy Issues* **1998**, *11* (1), 203–210.

(7) Gray, P. G. *Gas Sep. Purif.* **1993**, *7* (4), 213–224.

(8) Knoblauch, K. *Gas Sep. Purif.* **1993**, *7* (4), 195–196.

(9) Al-Marzouqi, M.; El-Naas, M.; Marzouk, S.; Abdullatif, N. *Sep. Purif. Technol.* **2008**, *62* (3), 499–506.

(10) Satyapal, S.; Filburn, T.; Trela, J.; Strange, J. *Energy Fuels* **2001**, *15* (2), 250–255.

(11) Chakma, A. *Energy Convers. Manage.* **1997**, *38* (Suppl. 1), S205–S209.

(12) Lackner, K. S.; Butt, D. P.; Wendt, C. H. *Energy Convers. Manage.* **1997**, *38* (Suppl. 1), S259–S264.

(13) Gottlicher, G.; Pruschek, R. *Energy Convers. Manage.* **1997**, *38* (Suppl. 1), S173–S178.

(14) Gaudernack, B.; Lynum, S. *Energy Convers. Manage.* **1997**, *38* (Suppl. 1), S165–S172.

(15) Meratla, Z. *Energy Convers. Manage.* **1997**, *38* (Suppl. 1), S147–S152.

(16) Jody, B. J.; Daniels, E. J.; Wolsky, A. M. *Energy Convers. Manage.* **1997**, *38* (Suppl. 1), S135–S140.

(17) Pino, J. A.; Garcia, J.; Martinez, M. A. *J. Essent. Oil Res.* **1996**, *8* (4), 373.

(18) Gadalla, M.; Olujie, Z.; De Rijke, A.; Jansens, P. J. *Energy (Oxford, U. K.)* **2006**, *31* (13), 2073.

(19) Nakabayashi, M.; Okabe, K.; Fujisawa, E.; Hirayama, Y.; Kazama, S.; Matsumiya, N.; Takagi, K.; Mano, H.; Haraya, K.; Kamizawa, C. *Energy Convers. Manage.* **1995**, *36* (6−9), 419–422.

(20) Hiarayama, Y.; Kazama, S.; Fujisawa, E.; Nakabayashi, M.; Matsumiya, N.; Takagi, K.; Okabe, K.; Mano, H.; Haraya, K.; Kamizawa, C. *Energy Convers. Manage.* **1995**, *36* (6−9), 435–438.

(21) Okabe, K.; Matsumiya, N.; Mano, H. *Sep. Purif. Technol.* **2007**, *57* (2), 242–249.

(22) Chung, S. J.; Park, J. H.; Li, D.; Ida, J. I.; Kumakiri, I.; Lin, J. Y. S. *Ind. Eng. Chem. Res.* **2005**, *44* (21), 7999–8006.

(23) Xomeritakis, G.; Tsai, C.-Y.; Brinker, C. J. *Sep. Purif. Technol.* **2005**, *42* (3), 249–257.

(24) Sada, E.; Kumazawa, H.; Wang, J. S.; Koizumi, M. *J. Appl. Polym. Sci.* **1992**, *45* (12), 2181–2186.

(25) Sridhar, S.; Veerapur, R. S.; Patil, M. B.; Gudasi, K. B.; Aminabhavi, T. M. *J. Appl. Polym. Sci.* **2007**, *106* (3), 1585–1594.

(26) Rhim, J.-W.; Chowdhury, G.; Takeshi, M. *J. Appl. Polym. Sci.* **2000**, *76* (5), 735–742.

(27) Hillock, A. M. W.; Koros, W. J. *Macromolecules* **2007**, *40* (3), 583–587.

(28) Pesiri, D. R.; Jorgensen, B.; Dye, R. C. *J. Membr. Sci.* **2003**, *218* (1−2), 11–18.

(29) Baker, R. W. *Ind. Eng. Chem. Res.* **2002**, *41* (6), 1393–1411.

(30) Pandey, P.; Chauhan, R. S. *Prog. Polym. Sci.* **2001**, *26* (6), 853–893.

(31) Tanaka, K.; Okamoto, K.-I. Structure and Transport Properties of Polyimides as Materials for Gas and Vapor Membrane Separation. In *Materials Science of Membranes for Gas and Vapour Separation*; Yampolskii, Y. P., Pinnau, I., Freeman, B. D., Eds.; John Wiley & Sons Ltd.: Hoboken, NJ, 2006; p 445.

(32) Favre, E. *J. Membr. Sci.* **2004**, *229* (1−2), 241–242.

(33) Wijmans, J. G.; Baker, R. W. *J. Membr. Sci.* **1995**, *107* (1−2), 1–21.

(34) Paul, D. R. *Sep. Purif. Rev.* **1976**, *5* (1), 33–50.

(35) Lonsdale, H. K. *J. Membr. Sci.* **1982**, *10* (2−3), 81–181.

(36) Koros, W. J.; Fleming, G. K. *J. Membr. Sci.* **1993**, *83* (1), 1–80.

(37) Koros, W. J.; Mahajan, R. *J. Membr. Sci.* **2000**, *175* (2), 181–196.

(38) Bos, A.; Pünt, I. G. M.; Wessling, M.; Strathmann, H. *J. Membr. Sci.* **1999**, *155* (1), 67–78.

(39) Shimazu, A.; Tukasa, M.; Shigeru, K.; Yasuo, I. *J. Polym. Sci., Part B: Polym. Phys.* **2003**, *41* (3), 308–318.

(40) Coleman, M. R.; Koros, W. J. *J. Polym. Sci., Part B: Polym. Phys.* **1994**, *32* (11), 1915–1926.

(41) Coleman, M. R.; Koros, W. J. *Macromolecules* **1997**, *30* (22), 6899–6905.

(42) Coleman, M. R.; Koros, W. J. *Macromolecules* **1999**, *32* (9), 3106–3113.

(43) Recio, R.; Palacio, L.; Pradanos, P.; Hernandez, A.; Lozano, A. E.; Marcos, A.; de la Campa, J. G.; de Abajo, J. *J. Membr. Sci.* **2007**, *293* (1−2), 22–28.

(44) Fuhrman, C.; Nutt, M.; Vichtovonga, K.; Coleman, M. R. *J. Appl. Polym. Sci.* **2004**, *91* (2), 1174–1182.

(45) Wind, J. D.; Sirard, S. M.; Paul, D. R.; Green, P. F.; Johnston, K. P.; Koros, W. J. *Macromolecules* **2003**, *36* (17), 6433–6441.

(46) Pfromm, P. H.; Koros, W. J. *Polymer* **1995**, *36* (12), 2379–2387.

(47) Kim, J. H.; Koros, W. J.; Paul, D. R. *Polymer* **2006**, *47* (9), 3104–3111.

(48) Wang, R.; Cao, C.; Chung, T.-S. *J. Membr. Sci.* **2002**, *198* (2), 259–271.

(49) Kim, K. J.; So, W.-W.; Moon, S. J. *Preparation of 6FDA-Based Polyimide Membranes for CO_2 Gas Separation*; 2004; Vol. *153*, pp 531−534.

(50) Kim, J. H.; Koros, W. J.; Paul, D. R. *J. Membr. Sci.* **2006**, *282* (1−2), 21–31.

(51) Kim, J. H.; Koros, W. J.; Paul, D. R. *J. Membr. Sci.* **2006**, *282* (1−2), 32–43.

(52) Kim, J. H.; Koros, W. J.; Paul, D. R. *Polymer* **2006**, *47* (9), 3094–3103.

(53) Kim, K. J.; Park, S.-H.; So, W.-W.; Ahn, D.-J.; Moon, S.-J. *J. Membr. Sci.* **2003**, *211* (1), 41–49.

(54) Kim, T.-H.; Koros, W. J.; Husk, G. R. *Sep. Sci. Technol.* **1988**, *23* (12), 1611–1626.

(55) Liu, Y.; Pan, C.; Ding, M.; Xu, J. *Polym. Int.* **1999**, *48* (9), 832–836.

(56) Staudt-Bickel, C.; Koros, W. J. *J. Membr. Sci.* **1999**, *155* (1), 145–154.

(57) Staudt-Bickel, C.; Koros, W. J. *J. Membr. Sci.* **2000**, *170* (2), 205–214.

(58) Wind, J. D.; Paul, D. R.; Koros, W. J. *J. Membr. Sci.* **2004**, *228* (2), 227–236.

(59) Hibshman, C.; Mager, M.; Marand, E. *J. Membr. Sci.* **2004**, *229* (1−2), 73–80.

(60) Yoshino, M.; Nakamura, S.; Kita, H.; Okamoto, K.-I.; Tanihara, N.; Kusuki, Y. *J. Membr. Sci.* **2003**, *212* (1−2), 13–27.

(61) Shimazu, A.; Miyazaki, T.; Ikeda, K. *J. Membr. Sci.* **2000**, *166* (1), 113–118.

(62) Heuchel, M.; Hofmann, D.; Pullumbi, P. *Macromolecules* **2004**, *37* (1), 201–214.

(63) Tanaka, K.; Kawai, T.; Kita, H.; Okamoto, K.-I.; Ito, Y. *Macromolecules* **2000**, *33* (15), 5513–5517.

(64) Kawakami, H.; Nakajima, K.; Shimizu, H.; Nagaoka, S. *J. Membr. Sci.* **2003**, *212* (1−2), 195–203.

(65) Iwase, M.; Sannomiya, A.; Nagaoka, S.; Suzuki, Y.; Iwaki, M.; Kawakami, H. *Macromolecules* **2004**, *37* (18), 6892–6897.

(66) Koron, A. *Kobunshi Ronbunshu* **1994**, *51* (4), 251–257.

(67) Fried, J. R.; Hu, N. *Polymer* **2003**, *44* (15), 4363–4372.

(68) Tanaka, K.; Taguchi, A.; Hao, J.; Kita, H.; Okamoto, K.-I. *J. Membr. Sci.* **1996**, *121* (2), 197–207.

(69) Matsui, S.; Sato, H.; Nakagawa, T. *J. Membr. Sci.* **1998**, *141* (1), 31–43.

(70) Islam, M. N.; Zhou, W.; Honda, T.; Tanaka, K.; Kita, H.; Okamoto, K.-I. *J. Membr. Sci.* **2005**, *261* (1−2), 17–26.

(71) Tanaka, K.; Masaaki, O.; Hiroyuki, T.; Hidetoshi, K.; Okamoto, K.-I. *J. Polym. Sci., Part B: Polym. Phys.* **1992**, *30* (8), 907–914.

(72) Brown, D.; Clarke, J. H. R.; Okuda, M.; Yamazaki, T. *J. Chem. Phys.* **1994**, *100* (8), 6011–6018.

(73) Pandiyan, S.; Brown, D.; van der Vegt, N. F. A.; Neyertz, S. *J. Polym. Sci., Part B: Polym. Phys.* **2009**, *47* (12), 1166–1180.

(74) Tanaka, K.; Kita, H.; Okamoto, K.-I. *J. Polym. Sci., Part B: Polym. Phys.* **1993**, *31* (9), 1127–1133.

(75) Cornelius, C. J.; Marand, E. *J. Membr. Sci.* **2002**, *202* (1−2), 97–118.

(76) Matsumoto, K.; Xu, P.; Nishikimi, T. *J. Membr. Sci.* **1993**, *81* (1−2), 15–22.
(77) in`t Veld, P. J.; Stone, M. T.; Truskett, T. M.; Sanchez, I. C. *J. Phys. Chem. B* **2000**, *104* (50), 12028–12034.
(78) Wang, X.-Y.; in 't Veld, P. J.; Lu, Y.; Freeman, B. D.; Sanchez, I. C. *Polymer* **2005**, *46* (21), 9155–9161.
(79) Hölck, O.; Heuchel, M.; Böhning, M.; Hofmann, D. *J. Polym. Sci., Part B: Polym. Phys.* **2008**, *46* (1), 59–71.
(80) McKechnie, J. I.; Brown, D.; Clarke, J. H. R. *Macromolecules* **1992**, *25* (5), 1562–1567.
(81) van der Vegt, N. F. A.; Briels, W. J.; Wessling, M.; Strathmann, H. *J. Chem. Phys.* **1999**, *110* (22), 11061–11069.
(82) Spyriouni, T.; Boulougoris, G. C.; Theodorou, D. N. *Macromolecules* **2009**, *42* (5), 1759–1769.
(83) Eslami, H.; Müller-Plathe, F. *Macromolecules* **2007**, *40* (17), 6413–6421.
(84) Costello, L. M.; Koros, W. J. *J. Polym. Sci., Part B: Polym. Phys.* **1995**, *33* (1), 135–146.
(85) Singh-Ghosal, A.; Koros, W. J. *Ind. Eng. Chem. Res.* **1999**, *38* (10), 3647–3654.
(86) Hibshman, C.; Cornelius, C. J.; Marand, E. *J. Membr. Sci.* **2003**, *211* (1), 25–40.
(87) Pechar, T. W.; Kim, S.; Vaughan, B.; Marand, E.; Tsapatsis, M.; Jeong, H. K.; Cornelius, C. J. *J. Membr. Sci.* **2006**, *277* (1−2), 195–202.
(88) Wessling, M.; Huisman, I.; Boomgaard, T. v. d.; Smolders, C. A. *J. Polym. Sci., Part B: Polym. Phys.* **1995**, *33* (9), 1371–1384.
(89) Duthie, X.; Kentish, S.; Powell, C.; Nagai, K.; Qiao, G.; Stevens, G. *J. Membr. Sci.* **2007**, *294* (1−2), 40–49.
(90) Thundyil, M. J.; Jois, Y. H.; Koros, W. J. *J. Membr. Sci.* **1999**, *152* (1), 29–40.
(91) Chung, T. S.; Cao, C.; Wang, R. *J. Polym. Sci., Part B: Polym. Phys.* **2004**, *42* (2), 354–364.
(92) Pechar, T. W.; Kim, S.; Vaughan, B.; Marand, E.; Baranauskas, V.; Riffle, J.; Jeong, H. K.; Tsapatsis, M. *J. Membr. Sci.* **2006**, *277* (1−2), 210–218.
(93) Niwa, M.; Kawakami, H.; Kanamori, T.; Shinbo, T.; Kaito, A.; Nagaoka, S. *Macromolecules* **2001**, *34* (26), 9039–9044.
(94) Yeom, C. K.; Lee, J. M.; Hong, Y. T.; Choi, K. Y.; Kim, S. C. *J. Membr. Sci.* **2000**, *166* (1), 71–83.
(95) Shimazu, A.; Tsukasa, M.; Masatoshi, M.; Kenichi, I. *J. Polym. Sci., Part B: Polym. Phys.* **2000**, *38* (19), 2525–2536.
(96) Neyertz, S.; Douanne, A.; Brown, D. *Macromolecules* **2005**, *38* (24), 10286–10298.
(97) Neyertz, S.; Douanne, A.; Brown, D. *J. Membr. Sci.* **2006**, *280* (1−2), 517–529.
(98) Neyertz, S. *Macromol. Theory Simul.* **2007**, *16* (5), 513–524.
(99) Neyertz, S. *Soft Mater.* **2007**, *4* (1), 15–83.
(100) Neyertz, S.; Brown, D. *Macromolecules* **2008**, *41* (7), 2711–2721.
(101) Neyertz, S.; Brown, D. *Macromolecules* **2009**, *42* (21), 8521–8533.
(102) Ben-Naim, A. *Molecular Theory of Solutions*; Oxford University Press: Oxford, UK, 2006; p 400.
(103) Ben-Naim, A.; Marcus, Y. *J. Chem. Phys.* **1984**, *81* (4), 2016–2027.
(104) Frenkel, D.; Smit, B. *Understanding Molecular Simulation: from Algorithms to Applications;* Academic Press: San Diego, 1996.
(105) Brown, D. The gmq User Manual Version 4, **2008**. Available at http://www.lmops.univ-savoie.fr/brown/gmq.html.
(106) Clark, M.; Cramer, R. D.III; van Opdenbosch, N. *J. Comput. Chem.* **1989**, *10* (8), 982–1012.
(107) Frisch, M. J.; Trucks, G. W.; Schlegel, H. B.; Scuseria, G. E.; Robb, M. A.; Cheeseman, J. R.; Montgomery, J. A.; Vreven, J. T.; Kudin, K. N.; Burant, J. C.; Millam, J. M.; Iyengar, S. S.; Tomasi, J.; Barone, V.; Mennucci, B.; Cossi, M.; Scalmani, G.; Rega, N.; Petersson, G. A.; Nakatsuji, H.; Hada, M.; Ehara, M.; Toyota, K.; Fukuda, R.; Hasegawa, J.; Ishida, M.; Nakajima, T.; Honda, Y.; Kitao, O.; Nakai, H.; Klene, M.; Li, X.; Knox, J. E.; Hratchian, H. P.; Cross, J. B.; Bakken, V.; Adamo, C.; Jaramillo, J.; Gomperts, R.; Stratmann, R. E.; Yazyev, O.; Austin, A. J.; Cammi, R.; Pomelli, C.; Ochterski, J. W.; Ayala, P. Y.; Morokuma, K.; Voth, G. A.; Salvador, P.; Dannenberg, J. J.; Zakrzewski, V. G.; Dapprich, S.; Daniels, A. D.; Strain, M. C.; Farkas, O.; Malick, D. K.; Rabuck, A. D.; Raghavachari, K.; Foresman, J. B.; Ortiz, J. V.; Cui, Q.; Baboul, A. G.; Clifford, S.; Cioslowski, J.; Stefanov, B. B.; Liu, G.; Liashenko, A.; Piskorz, P.; Komaromi, I.; Martin, R. L.; Fox, D. J.; Keith, T.; Al-Laham, M. A.; Peng, C. Y.; Nanayakkara, A.; Challacombe, M. P.; Gill, M. W.; Johnson, B.; Chen, W.; Wong, M. W.; Gonzalez, C.; Pople, J. A. *Gaussian 03*; Gaussian Inc.: Wallingford, CT, 2004.
(108) Zhang, Z.; Duan, Z. *J. Chem. Phys.* **2005**, *122* (21), 214507.
(109) Hammonds, K. D.; Ryckaert, J.-P. *Comput. Phys. Commun.* **1991**, *62* (2−3), 336–351.
(110) Ciccotti, G.; Ferrario, M.; Ryckaert, J. P. *Mol. Phys.* **1982**, *47* (6), 1253–1264.
(111) Babarao, R.; Jiang, J. *Langmuir* **2008**, *24* (10), 5474–5484.
(112) Milano, G.; Guerra, G.; Müller-Plathe, F. *Chem. Mater.* **2002**, *14* (7), 2977–2982.
(113) Müller-Plathe, F. *J. Chem. Phys.* **1995**, *103* (10), 4346–4351.
(114) Brown, D.; Clarke, J. H. R. *Comput. Phys. Commun.* **1991**, *62* (2−3), 360–369.
(115) Berendsen, H. J. C.; Postma, J. P. M.; van Gunsteren, W. F.; DiNola, A.; Haak, J. R. *J. Chem. Phys.* **1984**, *81* (8), 3684–3690.
(116) Ewald, P. P. *Ann. Phys.* **1921**, *369* (3), 253–287.
(117) Brown, D.; Neyertz, S. *Mol. Phys.* **1995**, *84* (3), 577–595.
(118) Span, R.; Wagner, W. *J. Phys. Chem. Ref. Data* **1996**, *25*, 1509–1596.
(119) Deitrick, G. L.; Scriven, L. E.; Davis, H. T. *J. Chem. Phys.* **1989**, *90* (4), 2370–2385.
(120) Domotor, G.; Hentschke, R. *J. Phys. Chem. B* **2004**, *108* (7), 2413–2417.
(121) Bondar, V. I.; Kamiya, Y.; Yampolskii, Y. P. *J. Polym. Sci., Part B: Polym. Phys.* **1996**, *34*, 369–378.
(122) Wind, J. D.; Staudt-Bickel, C.; Paul, D. R.; Koros, W. J. *Macromolecules* **2003**, *36* (6), 1882–1888.
(123) Müller-Plathe, F. *Macromolecules* **1991**, *24* (24), 6475–6479.
(124) Saiz, E.; Gonzalez, M. M. L.; Riande, E.; Guzman, J.; Compan, V. *Phys. Chem. Chem. Phys.* **2003**, *5*, 2862–2868.
(125) Iwai, Y.; Higashi, H.; Uchida, H.; Arai, Y. *Fluid Phase Equilib.* **1997**, *127* (1−2), 251–261.
(126) Waldman, M.; Hagler, A. T. *J. Comput. Chem.* **1993**, *14* (9), 1077–1084.
(127) Buckingham, A. D.; Disch, R. L. *Proc. R. Soc. London, Ser. A* **1963**, *273* (1353), 275–289.
(128) Stannet, V. T.; Koros, W. J.; Paul, D. R.; Lonsdale, H. K.; Baker, R. W. *Adv. Polym. Sci.* **1979**, *32*, 69.
(129) Joly, C.; Le Cerf, D.; Chappey, C.; Langevin, D.; Muller, G. *Sep. Purif. Technol.* **1999**, *16* (1), 47–54.
(130) Chang, K.-S.; Hsiung, C.-C.; Lin, C.-C.; Tung, K.-L. *J. Phys. Chem. B* **2009**, *113* (30), 10159−10169.
(131) Fu, Y.-J.; Hu, C.-C.; Qui, H.-Z.; Lee, K.-R.; Lai, J.-Y. *Sep. Purif. Technol.* **2008**, *62* (1), 175–182.
(132) Pfromm, P. H. The Impact of Physical Aging of Amorphous Glassy Polymers on Gas Separation Membranes. In *Materials Science of Membranes for Gas and Vapour Separation*; Yampolskii, Y. P., Pinnau, I., Freeman, B. D., Eds.; John Wiley & Sons Ltd.: Hoboken, NJ, 2006.
(133) Lin, W. H.; Chung, T.-S. *J. Membr. Sci.* **2001**, *186* (2), 183–193.
(134) Chan, A. H.; Paul, D. R. *Polym. Eng. Sci.* **1980**, *20* (1), 87–94.
(135) Wang, X.-Y.; Willmore, F. T.; Raharjo, R. D.; Wang, X.; Freeman, B. D.; Hill, A. J.; Sanchez, I. C. *J. Phys. Chem. B* **2006**, *110* (33), 16685–16693.
(136) Ismail, A. F.; Lorna, W. *Sep. Purif. Technol.* **2002**, *27* (3), 173–194.
(137) Böhning, M.; Springer, J. *Polymer* **1998**, *39* (21), 5183–5195.
(138) Wang, J.-S.; Kamiya, Y. *J. Membr. Sci.* **1995**, *98* (1−2), 69–76.
(139) Wang, J.-S.; Naito, Y.; Kamiya, Y. *J. Polym. Sci., Part B: Polym. Phys.* **1996**, *34* (12), 2027–2033.
(140) Wang, J.-S.; Kamiya, Y.; Naito, Y. *J. Polym. Sci., Part B: Polym. Phys.* **1998**, *36* (10), 1695–1702.
(141) Fleming, G. K.; Koros, W. J. *Macromolecules* **1986**, *19* (8), 2285–2291.
(142) Kirchheim, R. *Macromolecules* **1992**, *25* (25), 6952–6960.
(143) Kirchheim, R. *J. Polym. Sci., Part B: Polym. Phys.* **1993**, *31* (10), 1373–1382.
(144) Wind, J. D. Improving Polyimide Membrane Resistance to Carbon Dioxide Plasticization in Natural Gas Separations, Ph.D. Thesis, University of Texas, Austin, **2002**.
(145) Ponitsch, M.; Gotthardt, P.; Gruger, A.; Brion, H. G.; Kirchheim, R. *J. Polym. Sci., Part B: Polym. Phys.* **1997**, *35* (15), 2397–2408.
(146) Gruger, A.; Gotthardt, P.; Ponitsch, M.; Brion, H. G.; Kirchheim, R. *J. Polym. Sci., Part B: Polym. Phys.* **1998**, *36* (3), 483–494.
(147) Gotthardt, P.; Gruger, A.; Brion, H. G.; Plaetschke, R.; Kirchheim, R. *Macromolecules* **1997**, *30* (25), 8058–8065.